Stony Brook University

OFFICIAL COPY

The official electronic file of this thesis or dissertation is maintained by the University Libraries on behalf of The Graduate School at Stony Brook University.

© All Rights Reserved by Author.

Observation of natural domain structure in ferroelectric superlattices by Piezoresponse Force Microscopy

A Thesis Presented

by

Lukas Kuerten

to

The Graduate School

in Partial Fulfilment of the

Requirements

for the Degree of

Master of Arts

in

Physics

Stony Brook University

August 2012

Stony Brook University
The Graduate School

Lukas Kuerten

We, the thesis committe for the above candidate for the
Master of Arts degree, hereby recommend
acceptance of this thesis.

Matthew Dawber - Thesis Advisor
Assistant Professor, Department of Physics and Astronomy

Maria Victoria Fernandez-Serra
Assistant Professor, Department of Physics and Astronomy

Dong Su
Staff Scientist, Physics, Brookhaven National Laboratory

This thesis is accepted by the Graduate School.

Charles Taber
Interim Dean of the Graduate School

Abstract of the Thesis

Observation of natural domain structure in ferroelectric superlattices by Piezoresponse Force Microscopy

by

Lukas Kuerten

Master of Arts

in

Physics

Stony Brook University

2012

In this work, an investigation of the natural domain structure of superlattices of $PbTiO_3$ with $CaTiO_3$ or $SrTiO_3$ at various volume fractions is presented. Superlattices were grown on $SrTiO_3$ substrates via off-axis magnetron sputtering. The first indication of domain structure was found by X-ray diffraction. The naturally occurring domain structures are *a priori* not visible in Piezoresponse Force Microscopy (PFM) images of the surface taken with an Atomic Force Microscope (AFM). A custom-developed sequence of PFM lithography (i.e. writing patterns of polarization) and subsequent scans allows imaging of the natural domain structure and domain walls on the scale of tens of nanometers. This is the first time that real space images of this extremely fine domain structure have been obtained using PFM.

Contents

Acknowledgements

Firstly, I wish to thank my advisor, Matthew Dawber, for his valuable guidance and constant support of my work. It was a pleasure to work with somebody who has such deep and extensive knowledge in the field, but nonetheless has not lost his ability to joke about it. His understanding for my obligations outside the laboratory and his insistence when I would not listen made it possible to complete a Master's thesis in these six short months. Also I am indebted to my labmates, Sara Callori, John Sinsheimer, Benjamin Bein, Humed Yusuf and Julie Coraor for their patience with a beginner dabbling in experimental physics (except for the occasional passionate frustration). All these have been to me not only a boss or a colleague, but friends. They formed a very valuable part of my time spent in the United States

My gratitude goes equally to my other two committee members, Marivi Fernandez-Serra and Dong Su, for taking an interest in my research. Sven Aeschlimann helped with the section on Atomic Force Microscopy, even though he never expected it to end up in a Master's Thesis.

The entire year at Stony Brook was only made possible by a scholarship of the German Fulbright Commission. The participation in a Fulbright exchange program has been one of the most exciting times of my life so far through all the encounters with new people, new places, new cultures and new customs. I am also grateful for additional financial support to the Stony Brook Department of Physics and Astronomy and the Studienstiftung des Deutschen Volkes.

Chapter 1

Introduction

1.1 Motivation

Ferroelectric materials have found numerous applications in modern devices. Of particular use are their strong piezoelectric responses, high dielectrical constant and switchable polarization, which make them suitable for sensors/actuators, optical components and memory devices, respectively. Some of the most commonly used ferroelectrics are the solid solution Lead Zirconate Titanate (PZT) and Lithium Niobate.

Previous investigations (e.g. [1, 2]) have shown that the piezoelectric responses of ferroelectric materials can be significantly increased by submitting them to strain, which can, for example, be achieved by epitaxial deposition or combining them into a superlattice of materials with slightly differing lattice parameters.

As will be explained in section 1.4 , such superlattices should exhibit a natural domain structure similar to domains in ferromagnets. In this thesis, real-space observation of ferroelectric domain structure in ferroelectric superlattices using PFM (as opposed to observation in X-ray diffraction [3, 4]) is demonstrated for the first time.

1.2 Ferroelectrics

A ferroelectric is a material that shows spontaneous and reversible polarization. It is a well-known effect that a dielectric will become polarized under the influence of an external electric field. However, this polarization immediately disappears once the external field is turned off. The key property of ferroelectric materials is that they exhibit a spontaneous polarization even without the presence of an electric field. When subjected to a switching external electric field, the Polarization exhibits a hysteresis loop similar to ferromagnetic hysteresis, hence the name *ferro*electric.

If a material is ferroelectric, it is always also piezoelectric (i.e. a strain on the material produces a voltage and vice-versa) and pyroelectric (i.e. heating or cooling the material induces a voltage). Ferroelectricity and piezoelectricity are only present in crystal structures that are non-centrosymmetric because a polar crystal structure is necessary for a polar distribution of charge - i.e. a polarization.

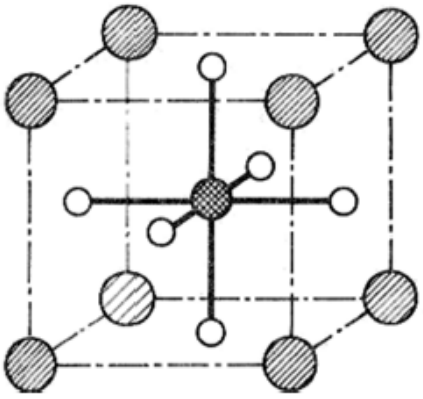

FIGURE 1.1: Unit cell of the Perovskite crystal structure. Dashed pattern signifies A-site atoms, grilled pattern B-site atoms and white signifies Oxygen atoms. (from [1])

Ferroelectricity was first found in Rochelle Salt (Potassium sodium tartrate $NaKC_4H_4O_6$), a complex molecule containing hydrogen bonds. Understanding and use of ferroelectrics was much stimulated by the discovery of ferroelectric behavior in the much more simple compound Barium Titanate ($BaTiO_3$). Like all materials investigated in the present work, $BaTiO_3$ is of Perovskite structure ABO_3, shown in Fig. 1.1 . Seen here is the ideal cubic perovskite structure, which is centrosymmetric and does not exhibit ferroelectricity. Fig. 1.2 shows more than one unit cell of the lattice, to elucidate the structure. Either

the A or the B atom may be defined as the center of a unit cell. At high temperatures, $BaTiO_3$ and other perovskites exist in a cubic paraelectric state:

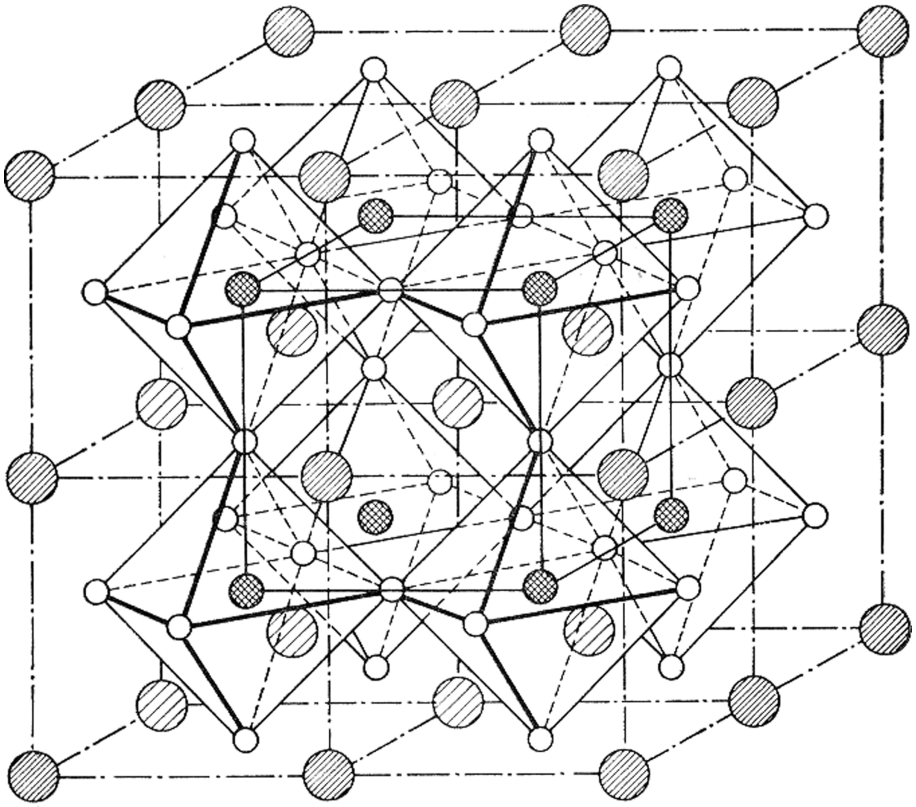

FIGURE 1.2: Larger Section of Perovskite structure (from [1])

Upon cooling below a transition temperature (393K for $BaTiO_3$, 760K for $PbTiO_3$ etc.), either the A or the B-site atoms shift from their positions. The result is a polar tetragonal crystal structure. The shifting atoms can move from their position in the cubic lattice either "'up"' or "'down"', this means the lattice has two stable configurations, i.e. a reversible polarization, signifying ferroelectricity. In Fig. 1.3 the cubic state and the tetragonal state in either of the two polarization directions is displayed for Barium Titanate as an example.

One of the perovskites investigated, $SrTiO_3$, does not have a ferroelectric phase at any temperature as a bulk material. Under compressive strain, however, ferroelectricity can be observed in this material [5]. Also, incorporation into a superlattice whith a ferroelectric material can force a polarization in $SrTiO_3$ for example, in combination with $BaTiO_3$ [6] or $PbTiO_3$ [7].

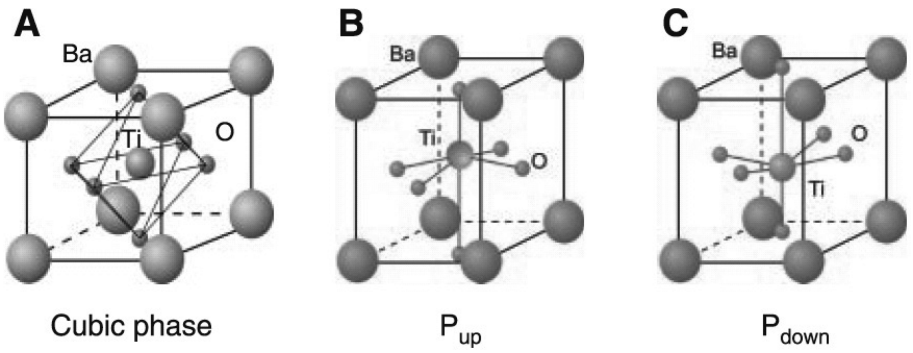

FIGURE 1.3: Barium Titanate Unit Cell in symmetric and polarized states (from [1])

Ferroelectricity in perovskites can occur in two variations, depending on the ionic radii. The two variations can be described based on the tolarance factor t,

$$t = \frac{r_A + r_B}{\sqrt{2}(r_B + r_O)} \tag{1.1}$$

with r_A and r_B the ionic radii of the A and B cations respectively and r_O the radius of the oxygen anion. The tolerance factor is an indication of the relative size of the ionic radii. A stable perovskite can only be formed with a set of given atoms, if their tolerance factor is approximately 1. If $t > 1$, the combined radii of A and O are so large that the space in the center of the unit cell is not completely filled by the B atom. Thus, the B atom can be displaced from its position at the center and create a ferroelectric polarization. This behavior is referred to as *B-site driven* ferroelectricity. Conversely, for $t < 1$, the A-site atoms are not completely confined between the oxygen octahedra and may thus move to generate a polarization.

In the materials in the present investigation (except $SrRuO_3$, which is not ferroelectric), Ti always occupies the B site.

For more details on ferroelectricity in perovskites, see e.g. [8]. As well as the ionic shift, displacement of the bound electrons in the material can have significant contributions to the polarization. Indeed, it has recently been found that in some materials the electronic contribution is significantly larger than the ionic contribution [9] .

1.3 Landau Theory of Ferroelectrics

For a theoretical description of the ferroelectric phase transitions, Landau theory is expedient. Landau theory is a phenomenological method to describe a thermodynamic system near a phase transition. One of its important assumptions is that a phase transition between two phases of different symmetry must be discontinuous. An "order parameter" is introduced which is zero in the higher-symmetry (i.e. disordered) phase and in the ordered phase approaches zero as approaching the phase transition. The free energy F of the ordered system is expressed as a power series in the order parameter - in the case of a transition between ferroelectricity and paraelectricity, the relevant order parameter is the spontaneous polarization $\mathbf{P}$: It is zero in the paraelectric phase, and in the ferroelectric phase approaches zero as the system approaches the transition temperature. Using Landau theory is a valid approach as long as changes in the order parameter are slow, a condition which is likely to break down very close to the phase transition - therefore, Landau Theory has to be employed cautiously. However, the interaction of electric dipoles has a significantly longer range than that of their magnetic counterparts, which means that the coordination number (the number of other dipoles that a given dipole interacts with) is high and Landau theory comparably stable.

A power series for F as a function of $\mathbf{P}$ can be expressed as (for simplicity, consider only $P =\mid \mathbf{P} \mid$)

$$F_P = \frac{1}{2}a_0(T - T_0)P^2 + \frac{1}{4}bP^4 + \frac{1}{6}P^6 - EP \tag{1.2}$$

Where E is the electric field. The form of temperature dependence of the first term is an assumption of the theory which has been verified by experiment. It shall be assumed that for the present purpose, a power series up to the sixth power is sufficient.

The equilibrium state of the system is at the minimum of the free energy:

$$\frac{\partial F_P}{\partial P} = 0 \tag{1.3}$$

In the paraelectric phase, the system has one minimum at $P = 0$. However, when the temperature falls below the transition temperature T_0, the form of the free energy changes

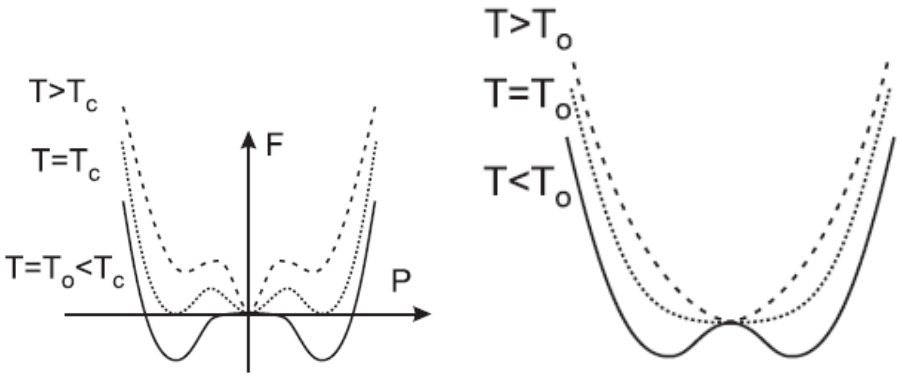

FIGURE 1.4: Free Energy as a function of Polarization at different temperatures for a first-order transition (left) and a second-order transition (right). When the temperature falls below T_C, a double-well develops, making spontaneous non-zero polarization the equilibrium state. (From [1])

into a double well potential with two minima at nonzero P. In Eq. 1.2 the coefficients a_0 and c are always positive, but the coefficient b may be either positive, so that the phase transition is of second order, or $b < 0$, then the phase transition is of second order. The difference between the two different modes of transition is illustrated in Fig. 1.4:

In the case of a first-order transition, the minimal point of the free energy jumps from P=0 to a P≠0 at T_C, consequently a discontinuity in the polarization appears at the phase transition. In the second-order case, the transition is continuous.

1.3.1 The influence of strain

In addition to the polarization, strain on a ferroelectric material also gives a considerable contribution to the free energy, which must consequently be included in the series expansion of F. Suppose a crystal is deformed by some external stress σ. The Strain Tensor η then gives the displacement $\mathbf{u}$ depending on the location $\mathbf{r}$ in the crystal. It is defined as:

$$\eta_{ij} = \frac{1}{2}\left(\frac{\partial u_i}{\partial r_j} + \frac{\partial u_i}{\partial r_i}\right) \tag{1.4}$$

When, as discussed earlier, a perovskite changes from cubic to tetragonal form, i.e. from paralectric to ferroelectric state, the deformation into a tetragonal lattice causes a

strain on the crystal. In that case, the leading order terms in the free energy from strain are:

$$F_\eta = \frac{1}{2}K\eta^2 + Q\eta P^2 + ... - \eta\sigma \tag{1.5}$$

Where K is the elastic constant of the material (i.e. the first term represents Hooke's law) and Q is a coefficient of strain-polarization-coupling . Now, to find the equilibrium state of the system, we need to minimize F with respect to both P and η. If we consider:

$$0 = \frac{\partial F(P,\eta)}{\partial \eta} = K\eta + QP^2 + ... - \sigma \tag{1.6}$$

and assume the material is not subject to external strains (σ= 0), then we find that the strain (in the case of a perovskite, the tetragonality) is proportional to P^2:

$$\eta = -\frac{QP^2}{K} \tag{1.7}$$

Through the profound effect that strain has on the crystal, it is often possible to significantly change the transition temperature for the ferroelectric/paraelectric transition.

This section is largely based on the corresponding chapter in [1] by Chandra and Littlewood.

1.4 Ferroelectric Domain Structure

Even though one has to be careful when drawing analogies between ferroelectric and ferro*magnetic* materials, in one respect both are alike: They form domains, i.e. microscopic regions in the material which have the same direction of polarization or magnetization, respectively. The reason for this is quite easy to see (even though the details can be rather tedious to calculate):

In a ferromagnet, the thermodynamically most stable configuration, i.e. the minimum of the free energy, is achieved when all magnetic moments are in parallel. However, for

a finite-size ferromagnetic this implies that the magnetic field will extend outside the material, which increases the energy in the system. The energy cost can be reduced by the formation of domains which have uniform magnetization in their interior, but are directed such that their magnetizations cancel each other. (See Fig. 1.5).

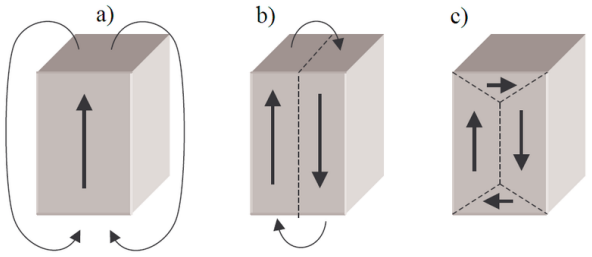

FIGURE 1.5: Reduction of external field and energy by formation of domains (from Wikipedia)

The situation with ferroelectric materials is similar in principle, but complicated by the fact that external electric fields may also be reduced by the accumulation of electric surface charge. Consider for example a capacitor consisting of two conducting electrodes. If a dielectric material is placed between the electrodes and a voltage applied, the dielectric is polarized, i.e. charges in the dielectric are displaced into opposite polarity of the charges in the electrodes. (See Fig. 1.6). If the voltage is taken away from the capacitor, the polarization in the dielectric also disappears. If, however, instead of a dielectric a ferroelectric is used, a remnant polarization remains, which causes charges to remain on the capacitor. If at the interface between ferroelectric and capacitor the number of bound charges in the ferroelectric is not equal to the number of free charges in the electrode, an electric field occurs which is referred to as "Depolarization Field". In leaky (i.e. not perfectly electrically insulating) samples, such charge accumulations and depolarization fields may even occur at the interfaces of domains within the film. Also, ferroelectric polarization is caused by a displacement of the ions, which will cause significant strain at interfaces between regions of different polarizations.

Another difference between ferroelectric and ferromagnetic domains is that the walls between the former are much thinner than between the latter. Because of the different nature of the interactions, ferroelectric domain walls can be thin down to only a few unit cells, which allows very dense writing of domains down to diameters of 20nm [10].

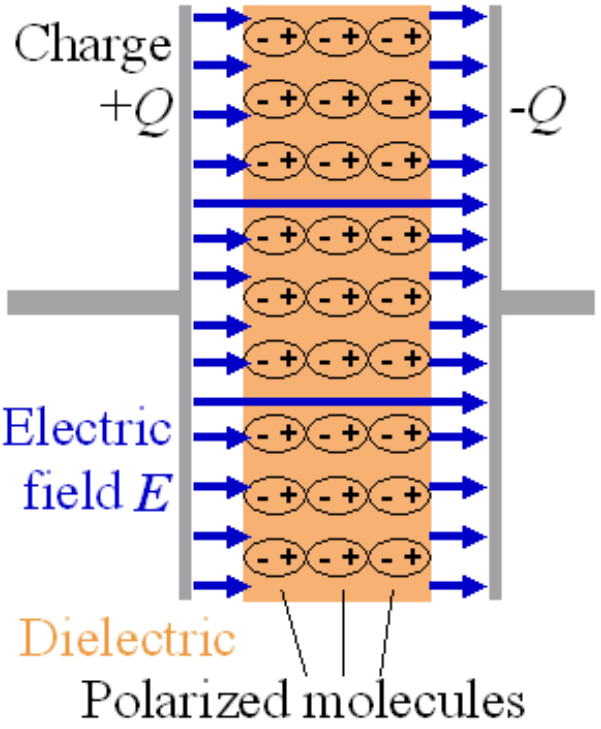

FIGURE 1.6: A capacitor with dielectric (from Wikipedia)

Under the influence of strain, ferroelectric materials form domains in the form of stripes with opposite polarization (180° domain walls). Such stripe domains have been theoretically predicted [11] and experimentally observed via X-Ray diffraction e.g. by [4, 12], and in one single case by topographic atomic force microscopy on PTO thin films [13] . The purpose of the present work is to image stripe domains on ferroelectric superlattices in real space using PFM for the first time. Ferroelectric domains (i.e. regions of uniform polarization) which have been artificially written with an AFM tip have been able to be readily produced and imaged for some time [14, 15] and have been more recently summarized in [16]. In the present investigation, we instead concentrate on the natural domain structure that is intrinsic in the material.

1.4.1 Polarization and piezoresponse at domain walls

The region between two domains is called a domain wall. Here, the polarization changes rapidly from the predominant direction in one adjacent domain to the direction of the other domain. In the aforementioned 180° regime, domain walls are very thin, typically

on the order of a few unit cells. The out-of-plane polarization and consequently the amplitude of the d_{33} piezoresponse is reduced in these domain walls, as can be easily seen from the vortex model for polarization which is demonstrated in Fig. 1.7.

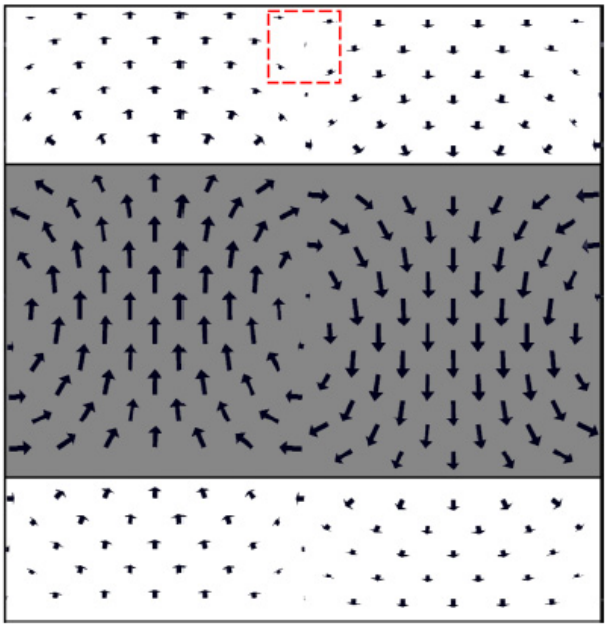

FIGURE 1.7: Simulation of the domain structure shows reduction of out-of-plane polarization at domain walls (from[7])

1.5 Ferroelectric superlattices and the influence of strain

In the present investigation, Lead Titanate ($PbTiO_3$, or shorter: PTO), forming one end of the PZT spectrum, is grown into superlattices with Calcium Titanate ($CaTiO_3$, CTO) or Strontium Titanate ($SrTiO_3$, STO). Substrates of $SrTiO_3$ with TiO_2 termination are used, on which a bottom electrode Strontium Ruthenate ($SrRuO_3$, SRO) with a thickness of usually 100nm is deposited before the superlattice deposition. Calculations on the influence of strain on thin-film PTO were performed earlier by [17]. More recent results on strained PTO/STO superlattices can be found in [7, 18].

The films were grown epitaxially onto the substrate, meaning that in the horizontal plane, the lattice parameters of the film are strained to be equal to those of the substrate.

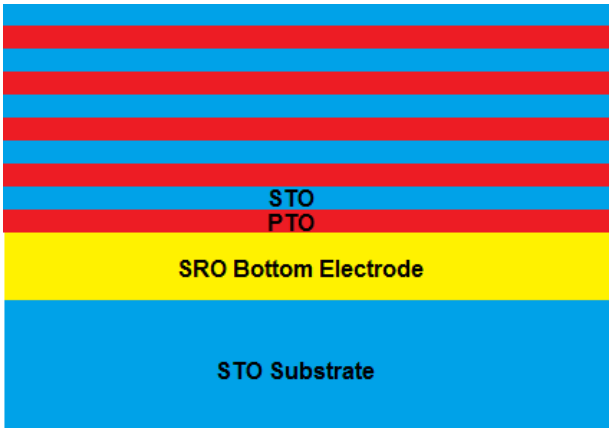

FIGURE 1.8: Schematic of a typical sample setup (not drawn to scale)

Since the unit cell sizes of $SrTiO_3$ and the film materials differ slightly (see Sec. 2.3), this means that the film materials are strained, in the present case they are compressed in the in-plane (horizontal) directions and consequently extended in the out-of-plane (vertical) direction. In Eq. 1.7 it was shown how the strain (more specifically, the tetragonality c/a) and the polarization of a film under no external stress are related. In a strained superlattice the relation remains similar which can shown in using the appropriate mixed boundary conditions of [17]:

$$\frac{c}{a} = \left(\frac{c}{a}\right)_0 + \text{constant} \cdot P^2 \tag{1.8}$$

When the film reaches a certain critical thickness, strain begins to relax through the formation of dislocations in the lattice and the desired strain effect is lost (See an in-depth discussion in [11]). This loss of tetragonality can be prevented by growing a superlattice of materials with different lattice parameters instead of a single film. For example, alternating thin films of $PbTiO_3$ and $SrTiO_3$ ensures that the $PbTiO_3$ is strained to the substrate lattice parameter of $SrTiO_3$ by each intermediate layer.

Furthermore, intrinsic size effects limit ferroelectricity in thin films. As was explained before, the perovskites under consideration can have either a centrosymmetric cubic structure which is favorable with regards to short-range forces. Or it can be in a ferroelectric tetragonal structure, which is favorable with regard to long-range interactions along the

polar axis. If now the size of the material along this polar axis falls below some critical length, the short-range interactions become dominant and ferroelectricity disappears. Fong et. al. found the minimal thickness for ferroelectricity in thin PTO films to be 3 unit cells [19].

Also, extrinsic size effects such as poor film quality or space charges near the surface may degrade the ferroelectricity of a thin film.

1.6 Previous results on PTO / STO Superlattices

Superlattices of ferroelectric (PTO) and dielectric (STO) materials have been thoroughly studied in the past. It has been found in lattices with sufficently high PTO volume fraction and STO layers not thicker than a few unit cells [20], that due to the high energy cost of a depolarization field at the ferroelectric/dielectric interface, polarization is approximately uniform throughout the material at a value between the polarizations of the two materials. This means that the ferroelectric polarization of the adjacent PTO layers forces the STO layers into a ferroelectric polarization as well and allows tuning the overall polarization thorugh the volume fraction. The polarization of a PTO/STO superlattice can be measured via the tetragonality c/a (see Eq. 1.8), which is directly accessible to x-ray measurements. These measurements and corresponding LDA-DFT calculations were found to be in good agreement.

The approach of tuning the ferroelectric properties of the superlattice through the PTO volume fraction was expanded in [18] and supplemented by electrical measurements. It was shown that the intermediate STO layers significantly reduce the leakage problems present in pure or solid-solution PTO samples. Also, an increase of the ferroelectric/paraelectric transition temperature of PTO by epitaxial strain was observed. These temperature measurements also showed that in a superlattice this phase transition is second-order, whereas it is first order in pure PTO.

In PTO/STO superlattices of very short periodicity (1/1 unit cells), it has been found ([2]) that instead of the polarizing change into a tetragonal structure, antiferrodistortive rotations of the oxygen atoms occur at the PTO/STO interfaces, which is referred to

as improper ferroelectricity. The influence of domain structures on the polarization was studied in [12].

Recent first-principles calculations on PTO/STO superlattices were performed by Aguado-Puente and Junquera [7]. They find that domain formation is isotropic, i.e. independent of the crystallographic orientation. The strong strain from ferroelectric distortions in PTO unit cells forces the adjacent STO layers to follow the displacement, thus the (normally paraelectric) STO is forced into a ferroelectric polarization.

1.7 Previous results on PTO / CTO Superlattices

In recent work, Sinsheimer et. al. [21] found that by combining lead titanate into superlattices with calcium titanate, the dielectric and piezoelectric coefficients of the superlattices at certain specific fractions of lead titanate are about double that of the bulk material.

The preferred direction of polarization for $PbTiO_3$ samples constrained to $SrTiO_3$ substrates is [001] [17], i.e. out-of-plane, whereas strained $CaTiO_3$ has polarization in the [110], i.e. in-plane direction. It was found that by varying the thickness of the superlattice layers, a rotation of the overall polarization of the film through an intermediate monoclinic phase with polarization oriented along [u0v] planes could be achieved. This polarization rotation is thought to be the origin of the enhanced piezoresponse as is the case in the solid solutions $Pb(Zn_{1/3}Nb_{2/3})O_3$-$PbTiO_3$ (PZN-PT) and $Pb(Mg_{1/3}Nb_{2/3})O_3$-$PbTiO_3$ (PMN-PT).

Important results of this investigation are summarized in Fig. 1.9.

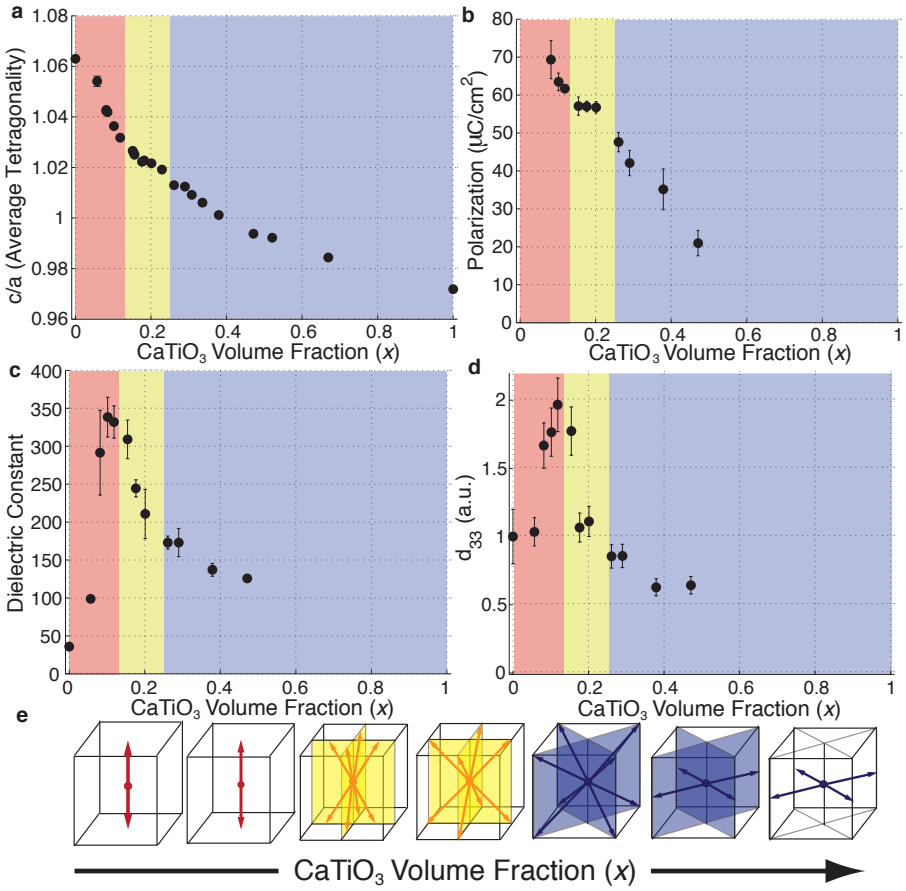

FIGURE 1.9: Variation of material properties for PTO/CTO-superlattices with volume fraction. The color shading indicates that the polarization of the film rotates from out-of-plane [001] (red) to in plane [u0v] (yellow) and then to [uuv] (blue). These directions of polarization are shown in the diagrams at the bottom. Samples for the present investigation were taken from the region of phase transition, where highest piezoelectric responses d_{33} occur. (from [21])

Chapter 2

Experimental Techniques

2.1 Deposition System

All films were grown in a custom-built vacuum chamber with off-axis magnetron sputter-deposition onto pre-manufactured $SrTiO_3$ substrates supplied by CrysTec.

2.1.1 Magnetron Sputter Deposition

Magnetron sputtering is a form of physical vapor deposition (PVD). PVD means that material is deposited on the substrate from a vapor phase in a vacuum chamber. In contrast to Chemical Vapor Deposition (CVD), the vapor is formed through physical processes and not by chemical reactions. Common methods of PVD are for example Molecular Beam Epitaxy, in which the deposition material is heated in a separate chamber (Knudsen Cell) and introduced into the vacuum chamber through a small opening, or erosion of a solid target by laser beams.

In sputtering, argon ions are accelerated towards a solid block of the material that is to be deposited (the target). Upon impact, the argon ions kinetically dislocate atoms or molecules from the target, which enter into the vapor phase and can then be deposited on the substrate. If the target consists of a compound of different elements (in our case e.g. $PbTiO_3$), the different constituents can be dislocated by the argon at different rates.

In this case, presputtering is necessary to ensure that the deposited film has the same stoichiometry as the target.

During pre-sputtering, the target is bombarded with argon, but no substrate placed in the chamber, so that the target is eroded, but no film is deposited. This insures correct stoichiometry of the vapor and erases unwanted dirt or oxides that may have settled on the target.

Argon ions hit the target at energies between 50eV and 1keV, which is high enough to strike out surface particles, but not so high that the cross section with the surface particles would significantly decrease. The ions are accelerated from a plasma to these energies due to an external electric field, that has the target as the cathode and the substrate and walls of the vacuum chamber as Anode. The charged Argon ions are accelerated by the field towards the target. The particles ejected from the target are predominantly electrically neutral, therefore the electric field does not confine them.

Since the perovskite materials used for our superlattices are electrical insulators, this basic "DC"-Approach to sputtering is not feasible in the present case, because positive charge would build up on the target. Therefore, a slightly more complex setup is used:

Instead of applying a DC bias between target and chamber, the target is connected to a radio frequency (RF) generator, while the chamber is grounded. This RF field between target and chamber first creates the plasma, i.e. it separates ions and electrons. The electrons follow the oscillations of the RF field, whereas the heavier Ar^+ ions stay in place. Because the target, serving as one "electrode" of the field, is much smaller than the other "electrode", i.e. the entire chamber except the target, the electron concentration near the target is increased, leading to a voltage that accelerates the Ar-ions towards the target.

The perovskites deposited in our experiment are oxides, and thus it is necessary to maintain a certain concentration of oxygen in the vacuum chamber to make sure they are incorporated into the film in their oxidized state. This introduces the additional complication, that Oxygen may form O^- ions, which are accelerated by the DC bias towards the sample. If this happens, the O^- ions would re-sputter the material that was already deposited. This problem is avoided by placing the substrate not opposite to the target, but at a 90° angle, which is called off-axis sputtering.

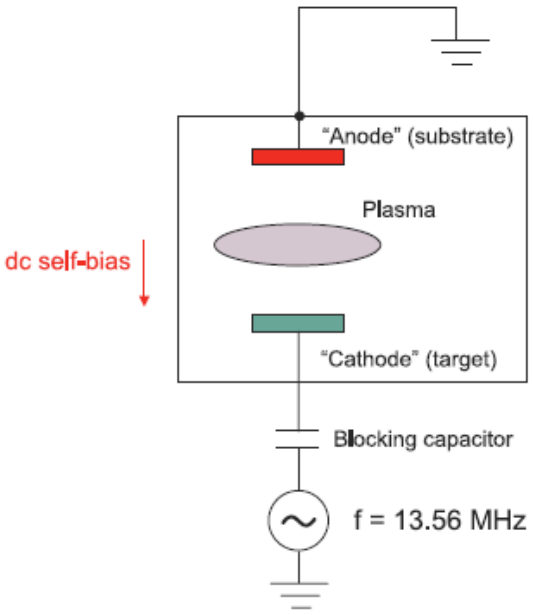

FIGURE 2.1: RF deposition system. (from [1])

Electrons are confined near the target by the toroidal magnetic field of a magnetron, which increases the self-bias and consequently the deposition rate.

The thickness of the grown films varies slightly with the different superlattices, since the thickness can only be a multiple of the respective periodicity, but all films are approximately 100nm thick.

More elaborate descriptions of the various deposition techniques feasible with ferroelectric thin films can be found in [1], on which this section is largely based.

2.1.2 Epitaxial Growth

Epitaxial growth means that the deposited film has the same crystal structure as the substrate on which it is grown. When the sputtered constituents of the film land on the substrate, they arrive at random positions. Only if they can move on the surface (diffusion) can they be incorporated into the growing film lattice and thus reach a stable minimum of energy. To increase the mobility of the atoms and facilitate the construction of the lattice, the substrate is heated during the deposition process. Surface diffusion

increases with temperature, thus a high temperature is desirable for growth of a smooth film. However, care has to be taken not to exceed temperatures where atoms begin to significantly diffuse into the bulk.

A perovskite contains oxygen, therefore a constant supply of oxygen has to be provided in the chamber to ensure that the material settles in the proper oxidation stage. The RF field in the chamber generating the argon plasma in the chamber also serves to break up O_2 molecules into atomic oxygen used for oxidation.

Precise control over the temperature of the sample was exercised at all times during the deposition process. In addition to the argon flow in the chamber necessary for sputter deposition, a controlled flow of oxygen was also supplied to ensure the correct formation of oxides.

For AFM measurements, samples were mounted on a copper plate. Since the $SrTiO_3$ substrate is isolating, electrical conductivity between the copper plate and the $SrRuO_3$ bottom electrode was facilitated by wire-bonding.

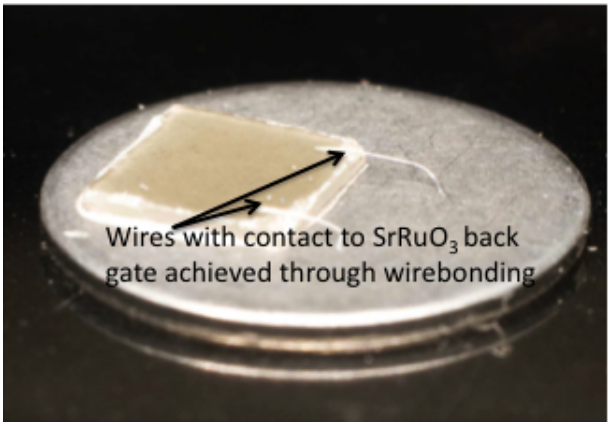

FIGURE 2.2: A sample wirebonded to a metal bottom-plate.

2.2 X-ray diffraction measurements

After deposition, all samples were thoroughly investigated by X-ray diffraction on a Bruker D8 Discover Diffractometer. X-ray-diffraction was used to ensure that lattice

parameters of the sample were grown as intended, in particular the thickness of the individual superlattice layers. It therefore serves as a measurement to calibrate growth rates and investigate tetragonality.

2.2.1 Observation of domains

Periodic domain structures in ferroelectric samples are visible as satellite peaks around the Bragg reflections of the film or superlattice in X-Ray diffraction measurements In epitaxial PTO thin films on STO, domain satellite peaks are observed around all Bragg peaks except those without out-of-plane components (hkl, l=0). This indicates a polarization exclusively in the out-of-plane direction with in-plane periodicity [4]. Results are similar on PTO/STO superlattices [12], see Fig. 2.3.

Results are different, however, on PTO/CTO superlattices. As mentioned in 1.7, the direction of the polarization is expected to rotate from the out-of-plane to the in-plane direction. This is supported by X-ray measurements which in this system show satellite peaks around Bragg peaks with out-of-plane components ((hkl), l≠0). Fig. 2.4 shows satellite peaks around the (100) and (110) substrate peaks on PTO/CTO superlattices of different volume fractions.

2.3 Materials

All the relevant Materials for Substrate, bottom electrode and film (superlattice) are of the perovskite structure, but they differ significantly in their properties.

- $SrTiO_3$

  Strontium titanate is the material used for all substrates in the present investigation. At room temperature, it is a cubic, paraelectric perovskite with lattice parameters a=b=c=3.905$\mathring{A}$. Below 110K, it changes into a tetragonal crystal structure, but ferroelectricity is suppressed by quantum fluctuations and does not appear at any temperature in the bulk. However, as was mentioned before, ferroelectrictiy at room temperature can be observed in strained STO and ferroelectricity can be induced when STO is combined with a ferroelectric material in a superlattice [7].

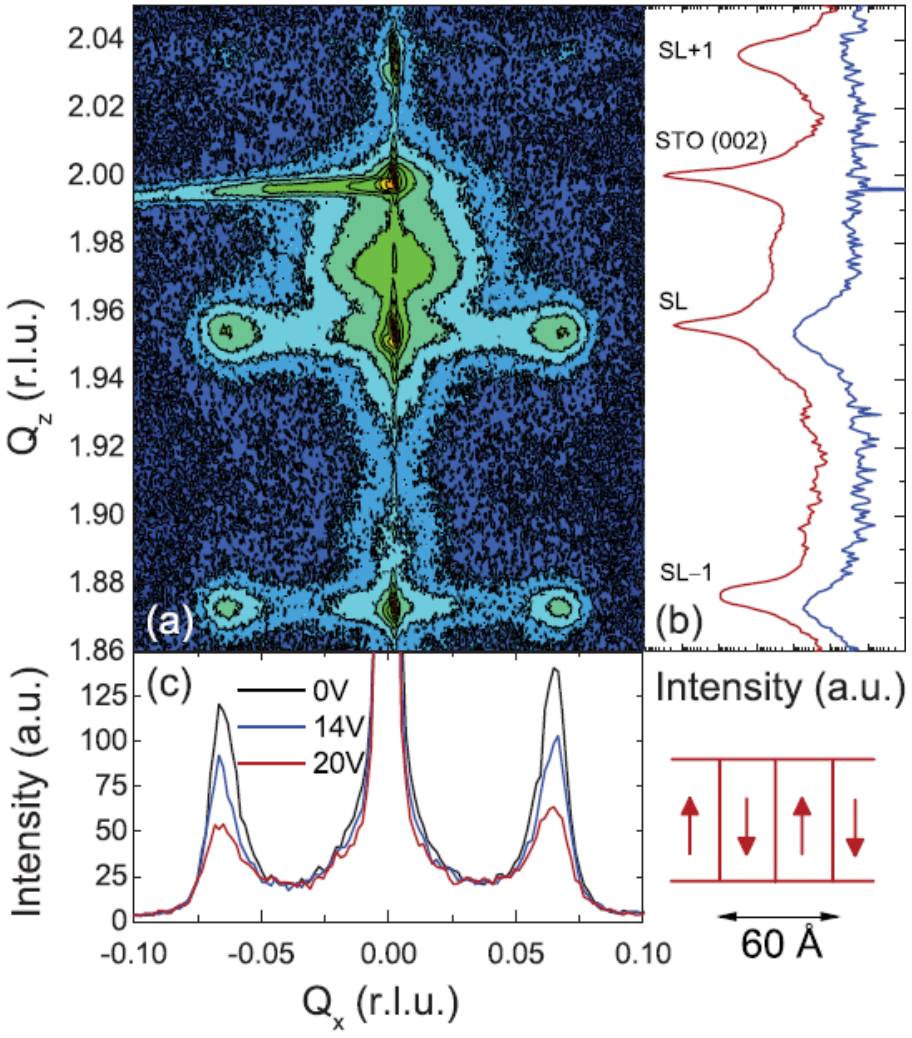

FIGURE 2.3: (a) Reciprocal space map around the STO (002) Bragg peak with three superlattice (SL) peaks, each SL peak with two domain satellite peaks. (b) Intensity profile of truncation rods through the Bragg peak at (002) (red) and through the satellite peaks (blue). (c) Variation of satellite peak intensity with applied external field.(from [22])

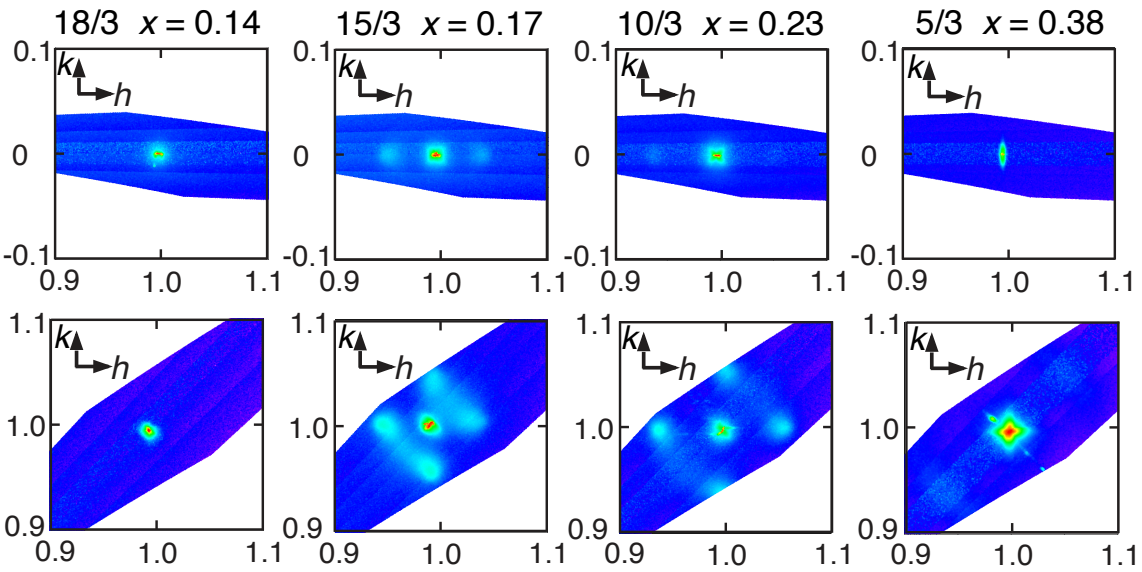

FIGURE 2.4: Reciprocal space maps around (100) (top row) and (110) (bottom row) substrate peaks obtained at grazing incidence. Satellite peaks due to domains are visible. Intensity is plotted on a logarithmic color scale. (from [21])

- $PbTiO_3$

  Lead titanate is a B-site ferroelectric at room temperature with a tetrahedral structure of a=b=3.904$\mathring{A}$. Above 760K, it is cubic and paraelectric (a=b=c=3.969$\mathring{A}$). It is commonly used in form of he solid solution Lead Zirconate Titanate (PZT), which shows strongly enhanced ferroelectricity compared to the pure material.

- $CaTiO_3$

  Calcium titanate is a dielectric perovskite. The crystal structure is orthorhombic with a=5.4412$\mathring{A}$, b=5.380$\mathring{A}$ and c=7.864$\mathring{A}$, but since the deviation from cubic is small, it may be regarded as pseudo-cubic with a=b=c=3.826$\mathring{A}$ [23].

- $SrRuO_3$

  Strontium ruthenate is a metallic perovskite, i.e. it is conducting and therefore used as a bottom electrode for ferroelectric films. The crystal structure is also orthorhombic with a=5.53$\mathring{A}$, b=5.57$\mathring{A}$ and c=7.85$\mathring{A}$, but like in CTO, it may be regarded as pseudo-cubic with a=b=c=3.93$\mathring{A}$. Thus, its lattice parameter matches the STO substrate sufficiently well to serve as electrode between substrate and film.

Chapter 3

Principles of Atomic Force Microscopy

3.1 Scanning Probe Microscopy (SPM)

In 1982 Binning and Rohrer presented the Scanning Tunneling Microcope (STM) [24] and thereby opened the way into a brand new world of microscopy: Scanning probe microscopy (SPM). Contrary to conventional microscopy mostly based on optical systems, the SPM uses a small sensor that is guided over the surface of the sample. During this scanning procedure, the sensor measures a designated physical criterion of the sample together with lateral x,y-coordinates. That way it is possible to create an electronic picture of the sample's surface.

By using piezoelectric crystals to move the detector, it is possible to control sensor movements on the Angstroem scale and to create pictures on the atomic scale. Since the development of the first STM the principle of the Scanning Probe Microscopy has been established as valuable tool in micro- and nanoanalytics. Different sensor types were developed to evaluate various surfaces.

3.1.1 Scanning Tunneling Microscopy (STM)

The STM uses a thin metallic needle as sensor, the tip of which can be as small as a single atom. A bias voltage between the sensor and the probe leads to a tunneling current that depends exponentially on the distance of the needle to the surface. There are two modes of operation: During the "constant current mode" the needle is guided over the surface and the height varied in such a way that the tunneling current stays constant. In another mode, the needle is guided over the surface at constant height. By measuring the variation of the current, a map of the topography of the probe is created. The major disadvantage of the STM is that it can only be used on conductive samples.

3.2 Atomic Force Microscopy (AFM)

The Atomic Force Microscope (AFM) was developed in 1986 by Binnig, Quate and Gerber. [25] It is the first SPM with which it was possible to display surfaces of nonconductive probes. In AFM, a tip of the size of down to a few nanometers is scanned over the sample to detect surface features. This tip is mounted on a cantilever, which is deflected as the tip moves over the sample. (Fig. 3.1). This cantilever deflection is measured and allows to record the surface measurement. The name *Atomic* Force Microscopy is due to the fact that repulsion or attraction between the tip and the sample surface is due to interactions between the respective atoms, which are enumerated in 3.2.2.

3.2.1 Measuring Cantilever Deflection

The cantilever deflection is the crucial measurement signal of the Scanning Force Microscope, thus, high precision is needed. At the same time, the measurement must not affect the deflection itself. In the history of the AFM many methods were employed. They ranged from making use of the tunneling effect to capacitive attributes of two electrodes. The method that is mostly used today (and also in the MFPD-3D Microscope employed in the present investigation) is the "laser beam deflection":

A laser beam that is pointed onto the cantilever is reflected onto a four-segment-photodiode (Fig. 3.1). Deflection of the cantilever leads to a change in the position of

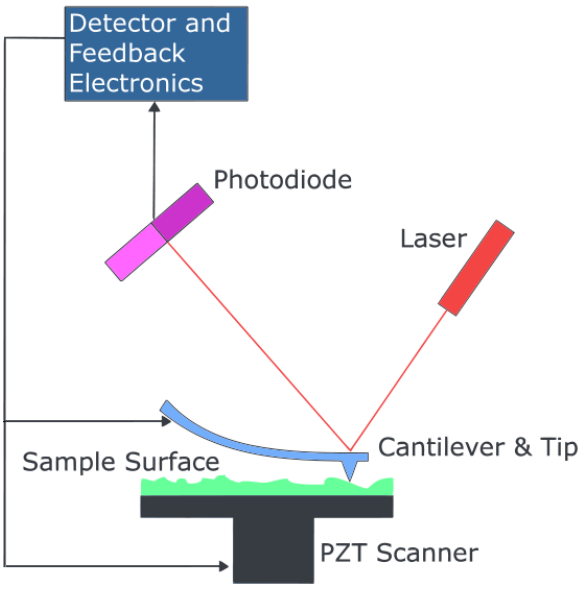

FIGURE 3.1: Sketch of the basic functional principle of an Atomic Force Microscope (from Wikipedia)

the reflected laser point on the photodiode. The resulting change of the signal of the four segments allows to track the cantilever deflection in the subangstroem scale. The T-B difference-signal is the voltage between the Top and Bottom segment and an indication for the topography of the surface. The L-R-Signal (left-right voltage) is an indication of the torsion of the cantilever. The torsion is due to lateral forces, mostly friction, when moving the tip over the sample surface.

The torsion is not completly independent of the deflection in the z-direction. Thus, the topography also affects the L-R-signal. We can distinguish friction forces from topography effects by changing the scanning direction, since the change of direction also changes the torsion of the cantilever. Friction of course only occurs when scanning in contact mode (see 3.2.3).

3.2.2 Forces between tip and sample

The interaction between the tip of the AFM and the sample surface includes several forces:

- van-der Waals interaction: attractive electrostatic dipole-dipole interaction between molecules
- capillary forces: attractive force resulting from a thin water film on the surface
- adhesion (only metallic samples): attractive force between metals when the objects are close enough to exchange electrons
- repulsive forces: when electronic orbits of two molecules overlap one another, the Pauli principle prohibits the electrons from occupying the same states. The consequence is a strong rise in potential energy when the molecules approach each other.

The van-der Waals interaction and the repulsive forces can be approximated by the Lennard-Jones-Potential:

$$V(z) = 4\epsilon \left((\frac{\sigma}{z})^{12} - (\frac{\sigma}{z})^{6} \right)$$

The Lennard-Jones Potential describes the interaction between two molecules. The interaction between the tip and the surface is a many-particle problem and thus, by far more complicated. The interaction combines all forces between the single atoms of the tip and the ones of the sample.

3.2.3 Topography Scanning Modes

The most basic use of an AFM is to scan the surface topography of a sample. This can be performed in two different "'modes"' (and several variations thereof):

- Contact mode

  During a contact mode measuremnt, the tip stays in contact with the surface at all times. The topography is recorded by the T-B-signal which is an indication of the cantilever's vertical bending. The tip is either guided over the sample in constant height ("constant height mode") or the height is constantly readjusted to keep the force approximately constant ("constant force mode"). This allows close tracking

of the surface, but degrades both tip and surface comparatively quickly. Also, in this mode the tip is subject to friction which may distort the measurement.

- Non-contact mode

  In non-contact mode (or AC-Mode), the tip is suspended closely above the surface, but does not touch it. The cantilever is excited to vibrations. While scanning over the surface, the forces between the tip and the sample surface change according to the changing distance between them. This then causes the resonance frequency and consequently the amplitude of the oscillations to change. Recording these variations of the amplitude allows to map the surface. In this mode, tip and surface are not degraded by scratching, and friction does not come into play. Thus it is usually the prefered mode for topography measurements.

3.2.4 Resolution

Just as the wavelength is the limiting factor of the resolution of an optical microscope, the AFM's resolution is mainly limited by the the fineness of the tip. A small radius of the tip is important to attain a high resolution, on the other hand it is sensitive and can easily be damaged. To achieve high definition on rough surfaces, a high aspect ratio, that means a small angle of the tip, is required. Fig. 3.2 shows the effect of the tip's size on the resolution.

3.2.5 Tips Used

All scans were performed with AFM tips supplied by MikroMasch. Topography scans were performed with NSC15 tips (325kHz, 46N/m). PFM requires a conductive coating of the tip, which tends to increase the tip radius. For scans on scales larger than 1μm, coated NSC18 (75kHz,3.5N/m) tips were used: Coatings for these Si-tips are available with Cr/Au, Ti/Pt, and Pt only. The Pt-only coating has the smallest tip radius of $<$ 25nm and yielded the best results of the three. For scans smaller than 1μm, the best choice are DPER18 (75kHz, 3.5N/m) tips with a Pt coating and a tip radius below 20nm.

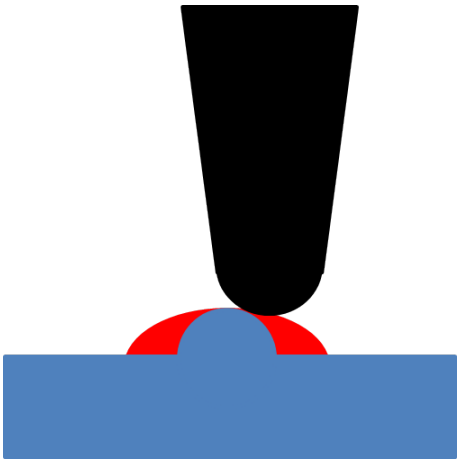

FIGURE 3.2: Effect of the tip size on resolution: Unless the tip (black) is significantly smaller than the surface feature (blue), the recorded signal (red) will be a convolution of the tip shape and the surface shape.

Chapter 4

Results from Piezoresponse Force Microscopy

4.1 Piezoresponse Force Microscopy (PFM)

Piezoresponse Force Microscopy is a variant of contact-mode Atomic Force Microscopy specifically designed for the investigation of piezoelectric samples and requiring the use of a tip and cantilever which are electrically conductive. An AC bias voltage is applied to the sample via the conductive tip, which induces oscillations in the piezoelectric material that is scanned. The tip is in contact with the surface and follows these oscillations which are detected by the AFM system. An early account of investigating ferroelectrics with custom-built PFM can be found in [15].

The Asylum Research MFP3D Atomic Force Microscope used in this investigation employs a special mode of PFM referred to as Dual Amplitude Resonance Tracking (DART): Since the piezoresponse is usually very weak (on the scale of pm), it is advisable to scan at the resonance frequency of the cantilever to achieve a maximum signal. However, in contact mode, the resonance frequency is not that of the cantilever alone, but of the combined system of cantilever, tip and surface. Since this frequency changes while scanning over the surface, it must be tracked to keep the frequency on the changing resonance peak. In DART mode, scanning at two frequencies, one on the left slope of the peak and one on the right slope of the peak, allows to lock-in the resonance and track it reliably.

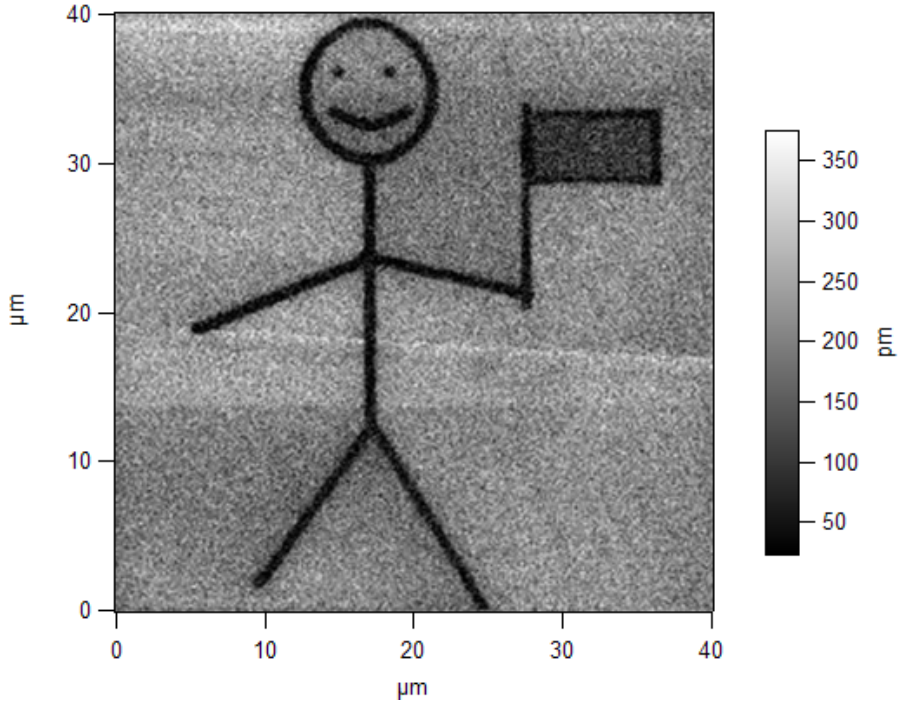

FIGURE 4.1: PFM gives clear and crisp results on a "large" scale (40μm in this case). It becomes increasingly difficult on smaller scales.

The amplitude at both frequencies is equal when both are at equal distance from the peak. When the resonance peak shifts in frequency, a difference between the two amplitudes emerges. By regulating the drive frequency always such that the difference in amplitudes remains zero, the resonance peak can be effectively tracked. (See Fig. 4.2) In particular, DART is expedient to eliminate most crosstalk coming from the topography of the sample.

The DART scanning mode records the vertical piezoresponse to a signal in the same direction: d_{33}. Measurement of the piezoresponse in other directions is considerably more difficult and could not be successfully demonstrated in the present investigation.

4.1.1 Measurement Channels in PFM

Scanning with DART PFM gives information on the sample surface in five different channels.

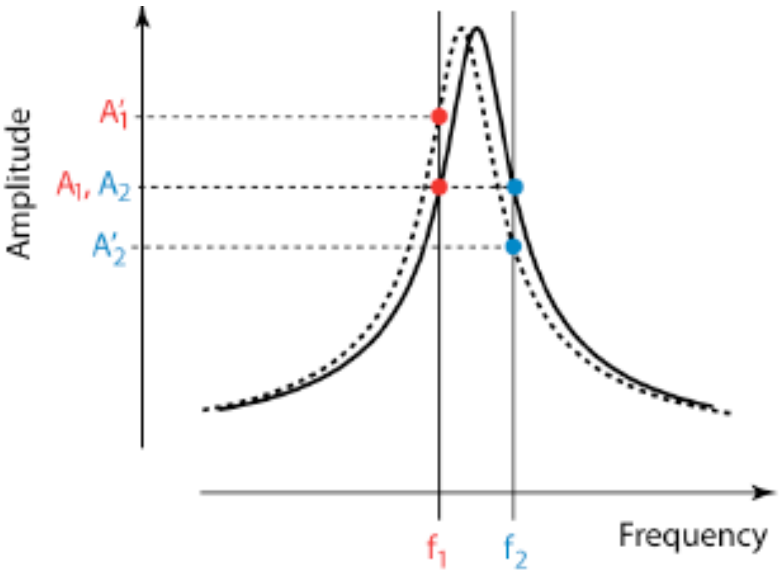

FIGURE 4.2: Principle of the DART tracking. A feedback loop regulates the frequencies f_1 and f_2 such that the difference between amplitudes A_1 and A_2 is always minimal, thereby ensuring that the resonance peak is always exactly in the middle.(From [26])

- Height

  While scanning in PFM mode, the topography is also always recorded. However, since the scan is done in contact mode and the tip size is comparatively large because of conductive coating, the topography image in PFM is typically less clear than images from designated non-contact topography measurements.

- Amplitude

  The amplitude of the oscillations in the cantilever-surface system, corresponding to the piezoelectric expansion and contraction of the surface, is recorded.

- Frequency

  The resonance frequency as tracked by the DART system is recorded.

- Phase 1 and Phase 2

  Phase is usually the most important signal in PFM measurements. It records the phase shift between the applied AC voltage (at two different frequencies in DART mode) and the piezoresponse of the sample. This phase shift corresponds to the

direction of the sample polarization: An applied electric field opposite to the polarization will cause an expansion of the sample. On the other hand, applying an electric field parallel to the polarization of the sample will make it shrink. This measurement channel is particularly useful since it is not as prone to crosstalk as the amplitude. Scanning at two drive frequencies in DART mode yields two phase signals.

4.1.2 Tip Size and limitations of accuracy

In the present investigations, different conductive AFM tips with sizes ranging from 15 to 50 nm were employed. However, the factual reliable resolution of these scans must be estimated more cautiously since voltages up to 20V were applied to the tips, so that the corresponding electric field will spread significantly wider than the actual tip size.

PFM images in literature tend to be on the length scales of several microns, which yields crisp and clear boundaries (see Fig. 4.1. However, on images at the length scale of tens of nanometers, tip size and spreading of the electric field tends to blur the edges of polarization regions. Investigations on a reference sample of Periodically Poled Lithium Niobate (PPLN) supplied by Asylum Research confirm that this blurriness is due to limitations of the measurement device and not an insufficiency of the sample.

A thorough discussion of the theory of resolution for PFM can be found in [10]. The two most important conclusions for the present work are:

- Since the width of 180° domain walls is known to be on the order of a few unit cells, i.e. a few nanometers, which is much smaller than the PFM resolution, the width of a 180° domain wall in the PFM image gives a good estimate of the resolution of that imaging process. Since we believe the observed domain walls to be of the 180° type, the width of domain walls in Fig. 4.7 and Fig. 4.9 shows that the resolution in the present investigation is about 10-20nm. This is may seem surprising, as it is slightly smaller than the radius of the AR DPER tip used to record the images, but:

- Features smaller than the resolution may still be visible, even though their intensity will be reduced as the smallness of the feature approaches the resolution.

For a report of writing nanoscale polarization regions on ferroelectrics, see e.g. [27].

4.1.3 Crosstalk with Topography

As mentioned earlier, the deformation of the sample under electric field is on the order of magnitude of picometers and therefore much smaller than the typical surface roughness of the sample. In particular, step edges resulting from mis-cut of the substrate have the height of one unit cell, approximately 4Å. Special care must be taken to rule out presumptive features in piezoresponse that are in reality only topography artifacts. Often, structures are found in the PFM images in the phase channels which are very similar to native domains, but can be identified as artifacts because they are exactly mirrored in the height image and/or because of their low phase contrast. Fig. 4.8 shows domain images in high intensity, below which a low-intensity feature is visible. This low-intensity signal has the same size and structure as a native domain, but due to its low intensity and by comparison with the height images, it can be identified as crosstalk.

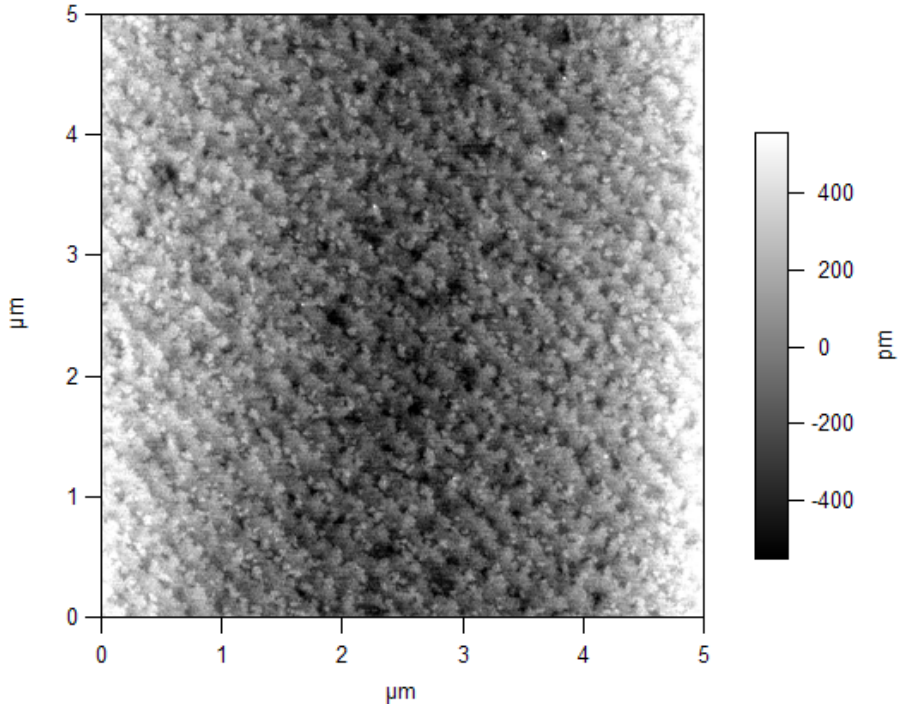

FIGURE 4.3: Step Edges on PTO/STO

4.2 Use of Lithography to discover native domain structure

The surface of the samples under consideration does not *a priori* show any domain structure. Features on the surfaces are measurement artifacts, most often crosstalk from the topography, and can be identified as such by comparison with the height image.

However, the surface can be primed by writing a uniform polarization on a certain area. The most successful method used in this investigation was to apply a negative bias voltage to a square with length of several hundred nanometers. For PTO/CTO samples, a bias of -10V is usually sufficient, whereas on PTO/STO samples usually -20V are required to switch the polarization. Higher voltages may improve the result, but can also irreversibly damage the film. Since negative polarity is the preferred direction of polarization of the material, writing with the a negative bias will leave a permanent, stable polarization. To the area surrounding the square, a positive bias (of the same voltage) may be applied to increase contrast at the borders. However, since this is contrary to the preferred direction of polarization, only a weak polarization will remain and the results differ only slightly from not applying a positive bias at all.

The polarization written in this way is stable towards deterioration over time, however it can be erased by scanning with high drive amplitudes or by lithography. Fig.4.5 shows a square written in lithography, of which a corner has been erased by consecutive scans at increasing voltages.

When an area has been primed by writing a constant bias voltage, one finds while scanning this area that the polarization in some regions is very stable, whereas it deteriorates very quickly (with scanning) in others. These areas of stable polarization have the size predicted by X-ray measurements for the native domain structures (a few tens of nanometers) and can thus be identified as domains.

Scanning domains at high drive amplitudes (approx. 10V) reveals the characteristic structure of domain walls in the amplitude channel.

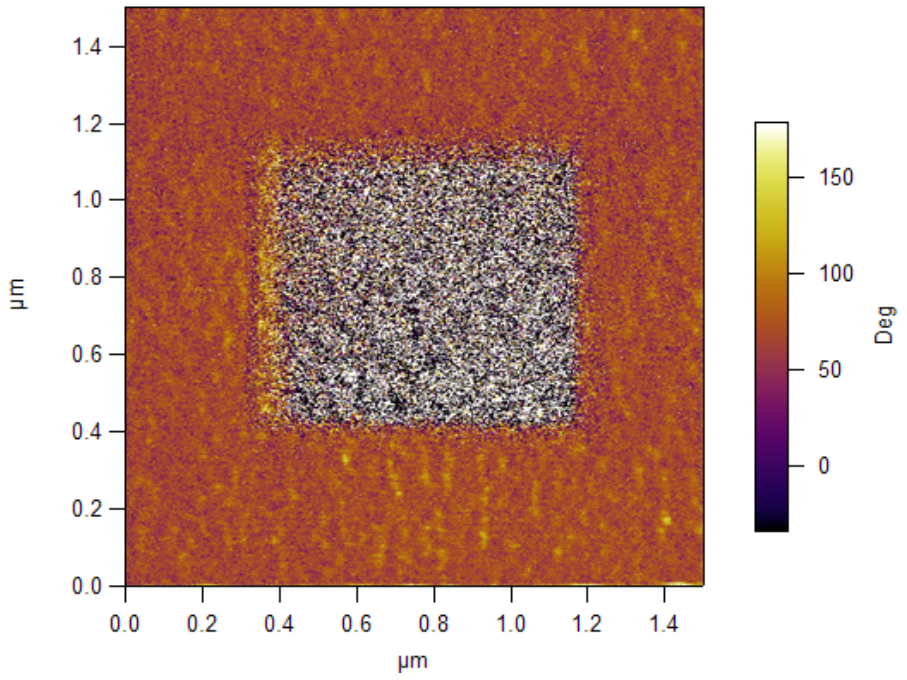

FIGURE 4.4: Square written on 24/3 PTO/CTO at 10V, scanned at 1V. The black-and white pattern seen here on the litho area is a measurement artifact due to insufficient tracking of the phase and disappears when doing close-up scans.

4.2.1 Observations on PTO/CTO superlattices

As a general rule, a sample's measured ferroelectric properties improve with the volume fraction of ferroelectric $PbTiO_3$. This is consistent with the results from [21]: In the measurements of this investigation, only the out-of-plane piezoresponse d_{33} was measured, which shows a distinct peak in Fig. 1.9 around the volume fraction corresponding to a 24/3 superlattice. (d_{33} is the coefficient of out-of-plane piezoresponse to out-of plane voltages.)

In the sample with lowest $PbTiO_3$ concentration of 9 unit cells of $PbTiO_3$ to 3 unit cells of $CaTiO_3$ (From now on denoted by the shorthand 9/3, 12/3 etc.), the polarization remaining after lithography is very weak. Domains are only very faintly visible, in most scans not perceivable at all.

On a 15/3 sample, lithography leaves a well-distinguishable image, even if the sample surface seems to consist of regions of different polarizability (which is true in different degrees for all samples investigated). Domains can be reproducibly found in the sample,

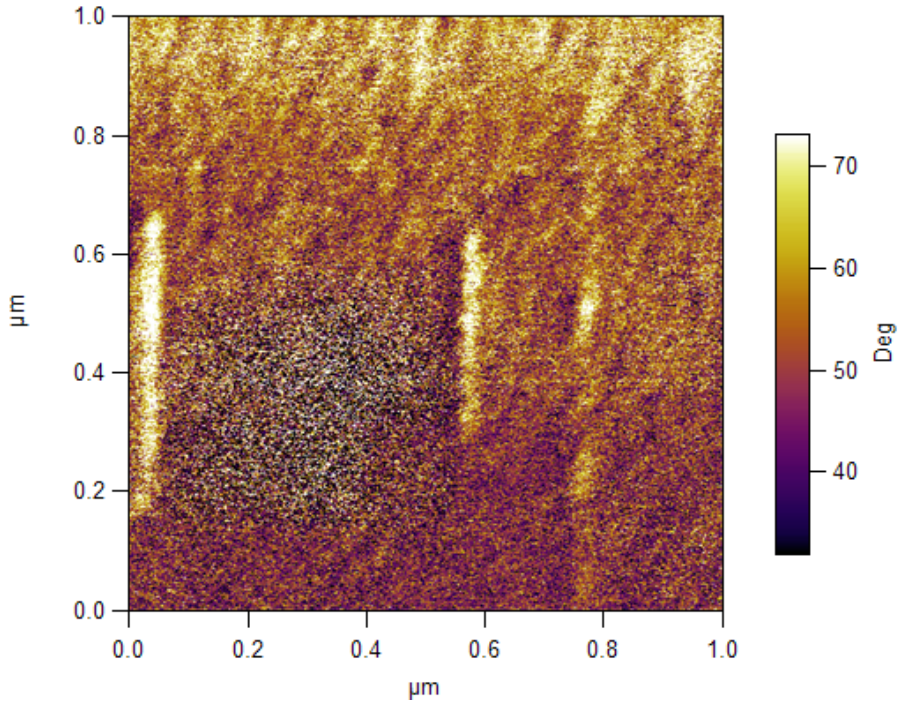

FIGURE 4.5: A lithography square in which the lower right corner has been erased by successive scans. For the comments on the white stripes, see section 4.2.4

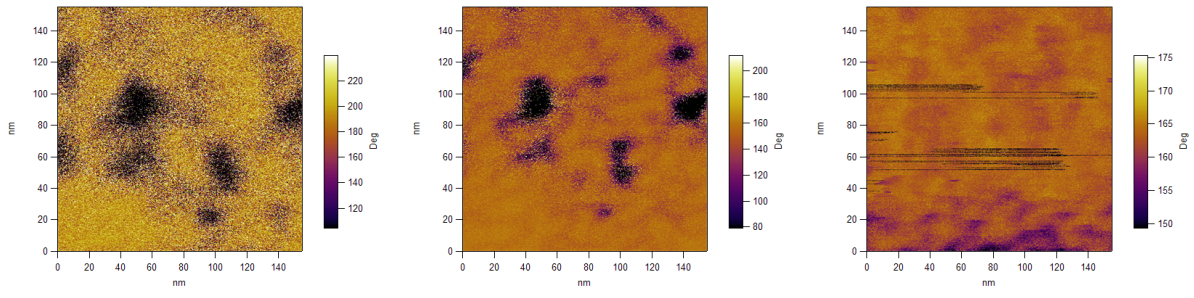

FIGURE 4.6: Three sequential close-up scans of an area with ferroelectric domains at increasing drive amplitude: Left: Scan at 2V shows indication of domain structure with stray polarization around it. Center: Scan at 5V has erased stray polarization, domains emerge clearly. Right: Scan at 10V has completely erased polarization in area, including domains.

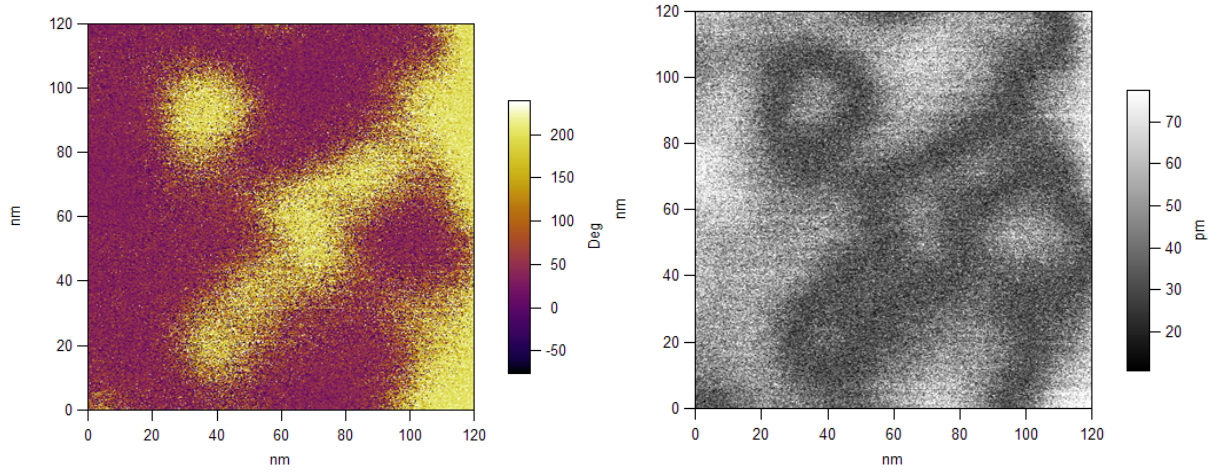

FIGURE 4.7: Phase (left) and Amplitude (right) Image of Domains on 15/3 PTO/CTO. Decreased Amplitude at domain walls is clearly visble.

but still care must be taken not to mistake them for crosstalk from the topography, because both show to approximately equal strength in the phase channel.

A 24/3 sample shows reliably good pictures from lithography. The images of domains in the phase channel are clearly distinguishable from crosstalk because they are of considerably higher magnitude. Often the predicted decrease in amplitude at domain walls can be observed. From the data of those scans, it is not yet possible to deduce the thickness of the domain walls, since the limiting factor is the size of the scanning tip.

Interestingly, some domains remain stable even when scanning at drive amplitudes of 10V, the voltage typically used for lithography, whereas others are erased while scanning at increasing drive amplitudes. The overall result that the 24/3-sample appears to be the most responsive to PFM of those samples investigated is concurrent with the results for d_{33} from [21]. Unfortunately, the rotation of polarization from out-of-plane to in-plane could not be investigated because the measurement technique for in-plane polarization, referred to as lateral PFM, could not yet be succesfully demonstrated with our setup. However, the fact that three colors of polarization appear in Fig. 4.9, in a sample of the volume fraction at which the polarization rotation occurs, indicates that the polarization is no longer constrained to the two up/down directions as it is in PTO/STO and at higher PTO volume fractions in PTO/CTO.

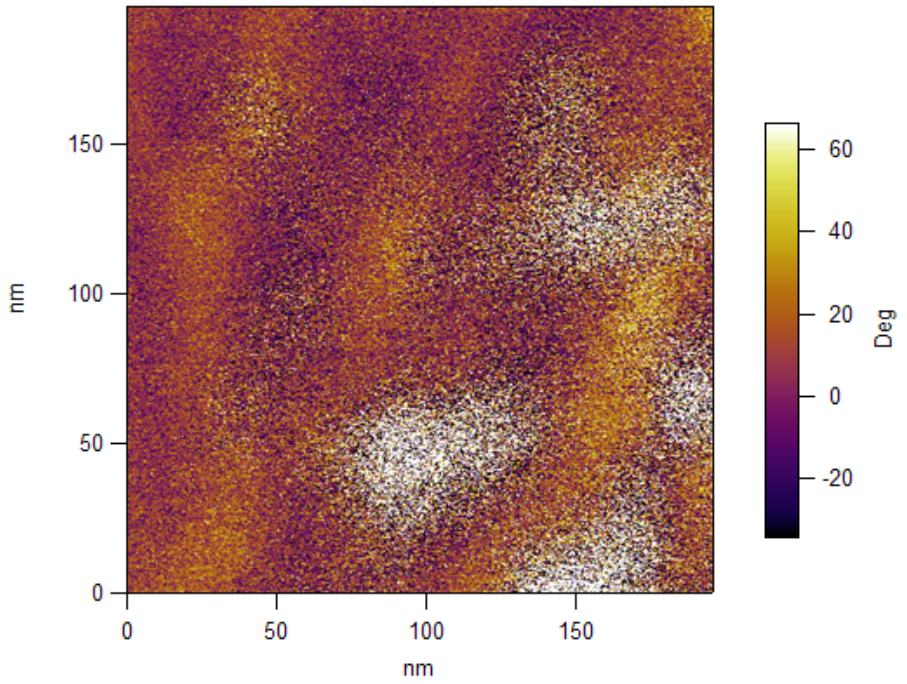

FIGURE 4.8: High-Intensity piezoresponse is clearly distinguishable from low-intensity topography crosstalk in 24/3 PTO/CTO sample

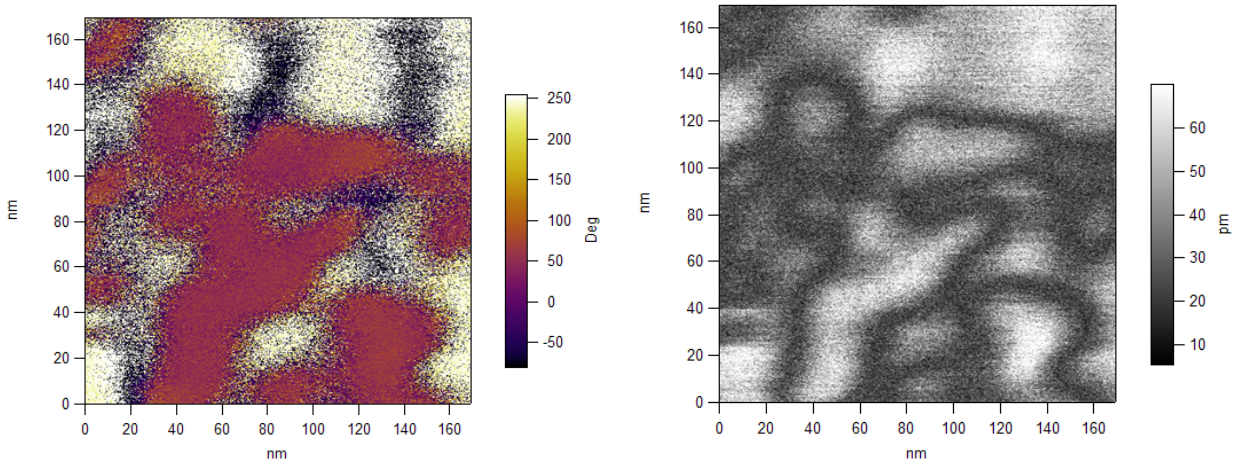

FIGURE 4.9: Phase (left) and Amplitude (right) Image of Domains on 24/3 PTO/CTO. Decreased Amplitude at domain walls is clearly visble. Note also the significantly higher phase contrast compared to 15/3 PTO/CTO.

4.2.2 Observations on PTO/STO superlattices

PTO/STO superlattices do not exhibit the polarization rotation that is present in PTO/STO, their polarization is expected to be exclusively out-of-plane. Thus, they make for a more reliable, but also less exciting subject. In terms of the method presented here, the first major difference to PTO/CTO is that switching of polarization generally occurs at higher voltages, thus lithograpy was performed at a -20V bias, sometimes even -30V which occasionally damages the film.

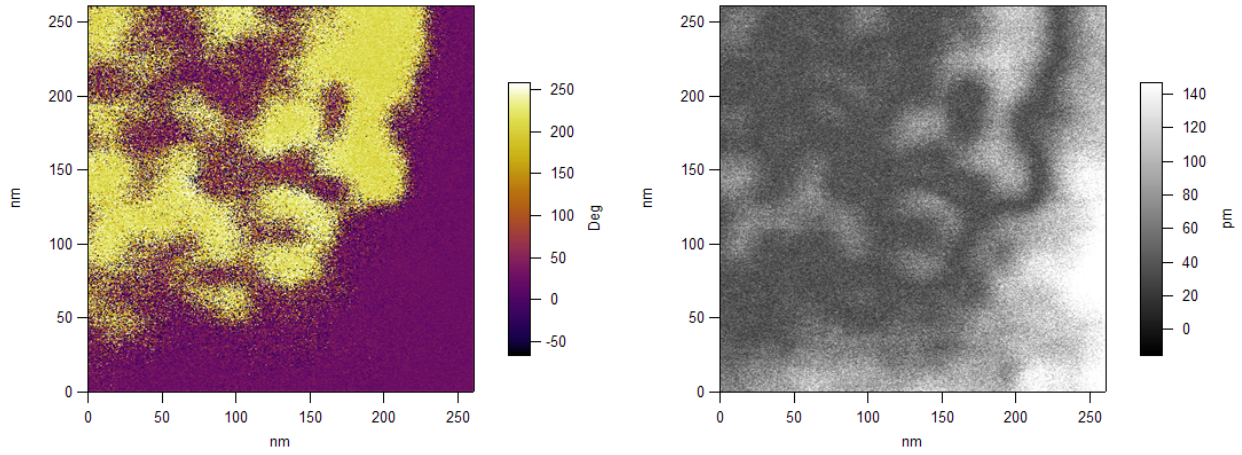

FIGURE 4.10: Phase (left) and Amplitude (right) Image of Domains on 18/3 PTO/STO. Decreased Amplitude at domain walls is clearly visible, note also the strong phase contrast which amounts to approximately 180°.

Higher switching voltages also infer that the domain structure is more stable, and accordingly, domains can be observed over the entire litho area in PTO/STO (see Fig. 4.11), whereas domains only appear in some regions of the litho area in PTO/CTO.

4.2.3 Observation of stripe domains

None of the features that could be identified as native domains were of the long-range ordered stripe structure that has been widely discussed in the literature. However, one has to keep in mind that all images recorded with PFM are only a 2D surface projection of the three-dimensional structure inside the superlattice. More importantly, the models in literature are usually observed either from first principles calculations with periodic

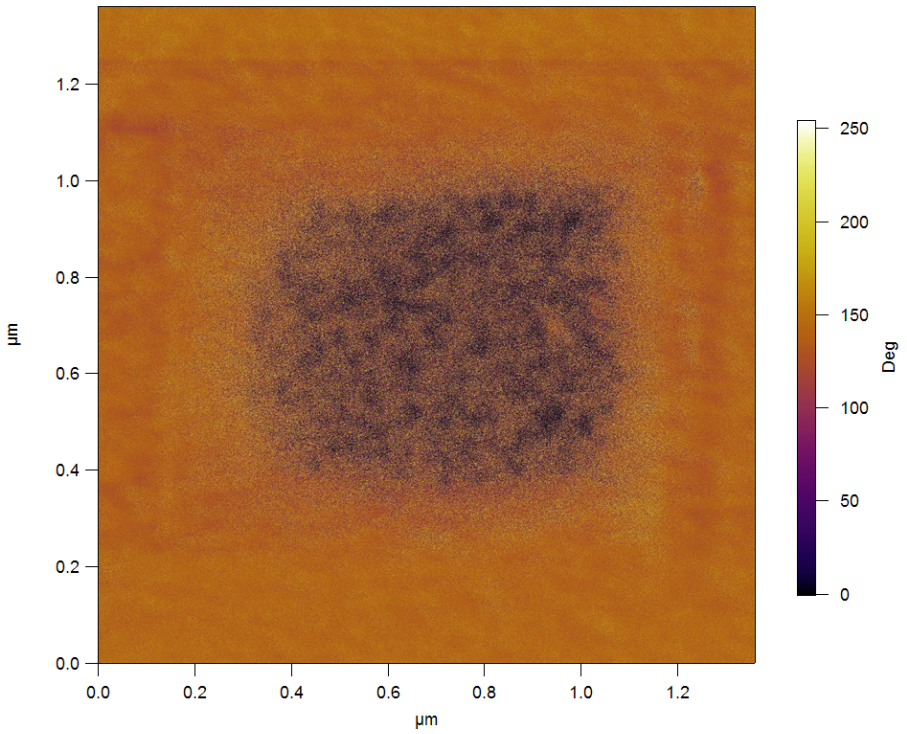

FIGURE 4.11: The entire Lithography area is covered in a pattern of domains on this 18/3 PTO/STO sample.

boundary conditions, or X-ray diffraction, which is only sensitive to periodic structures. It is possible that the domains are of a more complex periodicity - like a periodic arrangement of stripes in different directions shown in Fig. 4.12. The structures observed in PFM (reminiscent of a leopard patterning, see esp. Fig. 4.11) can be identified as a very irregular and distorted variant of this schematic.

If one assumes that the X-ray images only show the periodicity of the structure, while the irregularities are canceled, the results from X-ray and the present investigation are compatible. Another explanation may be, that the structure of domains is distorted at the surface and the AFM image registers these distortions, whereas the X-ray scans register mostly the pristine interior of the film.

The phase contrast between the observed domains is only very rarely a complete 180°. This is, however, no reason to rule out 180° domain walls, but rather can be due to many effects in the measurement process which reduce the observed phase contrast - for

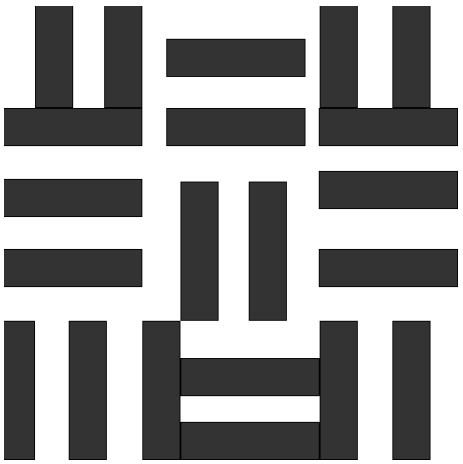

FIGURE 4.12: A proposed model for periodic arrangement of stripe domains

example, the top layer of the superlattices in the present investigation is STO, which is normally paraelectric.

4.2.4 White stripe artifacts

The white stripes on the side of the lithography square visible in Fig. 4.5 are a recurrent artifact. They appear along the slow scan direction, usually on one side of the square, sometimes on both. They are visible in the topography image as elevations of ≈800pm. A first assumption might be to dismiss them as a charging effect along the boundary of polarization, but the stripes are very stable over time, often more stable than the lithography image itself, which is atypical for charging effects. A second approach was to explain them as amounts of dust cleared from the lithography area, but the height of the stripes does not scale with the size of the lithography area as an amount of dust should. We have at the moment no conclusive explanation for this phenomenon.

Chapter 5

Conclusion and Outlook

For the first time, the existence of a native domain structure in ferroelectric superlattices has been demonstrated in real space using a specially designed sequence in Piezoresponse Force Microscopy. The dependence of the domain structure on the materials in the superlattices and their respective volume fractions has been detailed.

The present investigation is a concurrent approach to the previous investigations of domain structure via X-ray diffraction. Both methods have their intrinsic advantages and drawbacks:

- PFM gives direct information in the real-space domain, thus yielding results that are directly comprehensible to the naked eye, eliminating any need for Fourier analysis. However, since PFM is a scan only of the surface of the sample, results will be dominated by the surface properties of the material. In the context of ferroelectrics, screening charges immediately come to mind as measurement inhibitors. The fact that the predicted phase contrast of 180° was only very rarely observed in full may be attributed to this. Interpretation of the domain structure is especially difficult because PFM only shows a 2D projection of a 3D image.
- In X-ray diffraction, the entirety of the sample contributes to the material. However, reciprocal space maps in which domain peaks are observed may often be tricky to interpret. As was shown in the present work, the domain structure assumed to be highly ordered stripes from X-ray observation alone, is in fact considerably more complicated.

It is as of yet not entirely clear why a natural domain structure should not be visible in an unprimed sample. A plausible explanation is the model proposed by Jo et. al. in [28]: In the natural state, the piezoresponse of stripe domains is suppressed by electromechanical clamping: Under an applied electric field, adjacent domains of opposite polarization would undergo piezoelectric distortions into opposite directions, but these distortions are suppressed by lattice cohesion. The same paper proposes a mechanism of switching stripe domains into a uniform polarization state such that some regions of the sample remain in the striped state while others have already switched to uniform polarization. This explains our experimental data better than the alternative model proposed in [12].

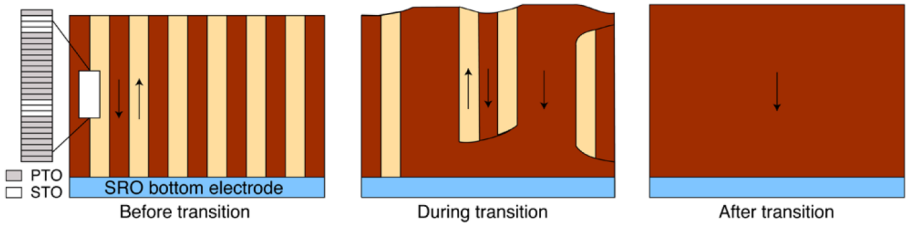

FIGURE 5.1: Proposed mechanism for heterogeneous switching of stripe domains (from [28])

The effect of priming the surface with a constant polarization is similar to what Jo et al. describe in their article [28]. Also the mechanism of switching domains proposed in the same paper is concurrent with the finding from the present investigation rather than the mechanism proposed in [12].

Our approach is similar to the earlier Ganpule experiment [29], which investigated domain formation and relaxation on PZT thin films. In contrast to Ganpule's samples, our materials have a preferred direction of polarization, but no uniform polarization in the as-grown state. Since the size of our domains is smaller than Ganpule's by more than an order of magnitude, consistent observation of the evolution over longer intervals of time is made difficult by thermal drift.

Observation of stripe domains on pure PTO thin films via atomic force microscopy was previously performed by Thompson et. al. [13]. They used tapping mode (i.e. topography) imaging techniques to detect the domain structure, which is observable due to minute differences in height between up- and down polarized regions and due to electrostatic effects. The results show stripe domains of thicknesses of a few nanometers

which are aligned either on step edges or on crystallographic features (see Fig. 5.2). The domain structures observed in the present work are slightly thicker ($\approx$ 20nm), but show neither the long-range coherence nor the alignment on step edges that was observed by Thompson et. al.

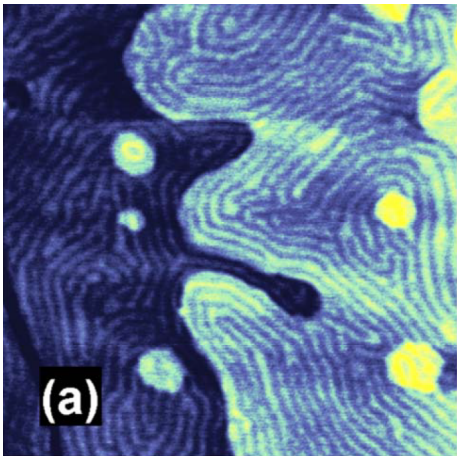

FIGURE 5.2: Long-range ordered stripe domains on pure PTO thin film aligned on step edges, observed by AFM topography measurement (from [13]).

Investigations by electron microscopy [30] were able to resolve the displacement of individual atoms in PTO/STO superlattices. Whereas TEM gives a sideways cross section of the domain structure, PFM gives a complimentary top view. An advantage of PFM over TEM is that a thin cross section of the sample does not have to be prepared, which besides being technically complicated and time consuming, may affect the domain structure of the sample.

In their investigation of domain switching in PTO/STO superlattices, Zubko et. al. [12] found that the domain structure returns to the original configuration even after being subjected to electric fields in excess of the coercive field. Long-term observations of domains are not possible with the present AFM method, since scans on such a small scale are subject to significant thermal drift. However, the stability of polarized domains at least over a few hours can be inferred from the observations.

The observed domains have a minimum thickness of $\approx$ 20nm in one dimension and are more elongated in the other direction. The size of the domains does not significantly depend on the relative thicknesses of the superlattice materials, nor on the interstitial material (STO or CTO). However, a thickness of 20nm is very close to the radius of the

employed AFM tips and it is very well possible that this observed thickness is due to limitations of resolution in the phase channel and the actual domain size is smaller. This view is particularly likely because in [21], presented in Fig. 2.4, a dependence of the domain satellite peak locations on volume fraction was observed.

It was shown that in PTO/CTO superlattices the out-of-plane polarization becomes more stable and the domain structure more pronounced with increasing PTO volume fraction. In PTO/STO, this trend was not predicted to be as pronounced as in PTO/CTO and could not be observed.

PFM Scans of pure PTO thin films were not conducted in the present investigation due to lack of time, but would be an essential next step to better understand the domain structure in these samples. Also, inverting the order of the superlattice deposition may improve PFM results: In this investigation, all superlattices were grown such that the lowest layer is PTO and the top layer is STO. A top layer of ferroelectric PTO may lead to a clearer domain image.

Bibliography

[1] K. Rabe, Ch. H. Ahn, and J. M. Triscone, editors. *Physics of Ferroelectrics - A Modern Perspective*, volume 105 of *Topics in Applied Physics*. Springer-Verlag, 2007.

[2] Eric Bousquet, Matthew Dawber, Nicolas Stucki, Celine Lichtensteiger, Patrick Hermet, Stefano Gariglio, Jean-Marc Triscone, and Philippe Ghosez. Improper ferroelectricity in perovskite oxide artificial superlattices. *nature*, 452:732–736, 2008. doi: 10.1038/nature06817. URL `http://www.nature.com/nature/journal/v452/n7188/full/nature06817.html?free=2`.

[3] S. J. Callori, J. Gabel, D. Su, J. Sinsheimer, M. V. Fernandez-Serra, and M. Dawber. Ferroelectric pto/sto superlattices with broken inversion symmetry. *Phys. Rev. Lett.*, in press.

[4] S. K. Streiffer, J. A. Eastman, D. D. Fong, Carol Thompson, A. Munkholm, M. V. Ramana Murty, O. Auciello, G. R. Bai, and G. B. Stephenson. Observation of nanoscale 180° stripe domains in ferroelectric pbtio$_3$ thin films. *Phys. Rev. Lett.*, 89: 067601, Jul 2002. doi: 10.1103/PhysRevLett.89.067601. URL `http://link.aps.org/doi/10.1103/PhysRevLett.89.067601`.

[5] J. H. Haeni, P. Irvin, W. Chang, R. Uecker, P. Reiche, Y. L. Li, S. Choudhury, W. Tian, M. E. Hawley, B. Craigo, A. K. Tagantsev, X. Q. Pan, S. K. Streiffer, L. Q. Chen, S. W. Kirchoefer, J. Levy, and D. G. Schlom. Room-temperature ferroelectricity in strained srtio3. *Nature*, 430:758–761, 2004. doi: 10.1038/nature02773. URL `http://www.nature.com/nature/journal/v430/n7001/full/nature02773.html?free=2`.

[6] J. B. Neaton and K. M. Rabe. Theory of polarization enhancement in epitaxial batio[sub 3]/srtio[sub 3] superlattices. *Applied Physics Letters*, 82(10):1586–1588, 2003. doi: 10.1063/1.1559651. URL http://link.aip.org/link/?APL/82/1586/1.

[7] Pablo Aguado-Puente and Javier Junquera. Structural and energetic properties of domains in $pbtio_3/srtio_3$ superlattices from first principles. *Phys. Rev. B*, 85:184105, May 2012. doi: 10.1103/PhysRevB.85.184105. URL http://link.aps.org/doi/10.1103/PhysRevB.85.184105.

[8] R. E. Cohen. Origin of ferroelectricity in perovskite oxides. *Nature*, 358:136, 1992. doi: 10.1038/358136a0. URL http://www.nature.com/nature/journal/v358/n6382/pdf/358136a0.pdf.

[9] Kensuke Kobayashi, Sachio Horiuchi, Reiji Kumai, Fumitaka Kagawa, Youichi Murakami, and Yoshinori Tokura. Electronic ferroelectricity in a molecular crystal with large polarization directing antiparallel to ionic displacement. *Phys. Rev. Lett.*, 108:237601, Jun 2012. doi: 10.1103/PhysRevLett.108.237601. URL http://link.aps.org/doi/10.1103/PhysRevLett.108.237601.

[10] S. V. Kalinin, S Jesse, B J Rodriguez, J Shin, A P Baddorf, H N Lee, A Borisevich, and S J Pennycook. Spatial resolution, information limit, and contrast transfer in piezoresponse force microscopy. *Nanotechnology*, 17:3400–3411, 2006. doi: doi:10.1088/0957-4484/17/14/010. URL http://iopscience.iop.org/0957-4484/17/14/010.

[11] J. S. Speck and W. Pompe. Domain configurations due to multiple misfit relaxation mechanisms in epitaxial ferroelectric thin films. i. theory. *J. Appl. Phys.*, 76, 1994. doi: 10.1063/1.357097.

[12] P. Zubko, N. Stucki, C. Lichtensteiger, and J.-M. Triscone. X-ray diffraction studies of 180 degree ferroelectric domains in $pbtio_3/srtio_3$ superlattices under an applied electric field. *Phys. Rev. Lett.*, 104:187601, May 2010. doi: 10.1103/PhysRevLett.104.187601. URL http://link.aps.org/doi/10.1103/PhysRevLett.104.187601.

[13] Carol Thompson, D. D. Fong, R. V. Wang, F. Jiang, S. K. Streiffer, K. Latifi, J. A. Eastman, P. H. Fuoss, and G. B. Stephenson. Imaging and alignment of nanoscale 180[degree] stripe domains in ferroelectric thin films. *Applied Physics Letters*, 93(18):

182901, 2008. doi: 10.1063/1.3013512. URL http://link.aip.org/link/?APL/93/182901/1.

[14] C. H. Ahn, T. Tybell, L. Antognazza, K. Char, R. H. Hammond, M. R. Beasley, . Fischer, and J.-M. Triscone. Local, nonvolatile electronic writing of epitaxial pb(zr0.52ti0.48)o3/srruo3 heterostructures. *Science*, 276(5315):1100–1103, 1997. doi: 10.1126/science.276.5315.1100. URL http://www.sciencemag.org/content/276/5315/1100.abstract.

[15] Oleg Kolosov, Alexei Gruverman, Jun Hatano, Takahashi Koichiro, and Hiroshi Tokumoto. Nanoscale visualization and control of frerroelectric domains by atomic force microscopy. *Phys. Rev. Lett.*, 74(21), 1995.

[16] E. Soergel. Visualization of ferroelectric domains in bulk single crystals. *Appl. Phys. B*, 81:729752, Oct 2005. doi: 10.1007/s00340-005-1989-9.

[17] N. A. Pertsev, A. G. Zembilgotov, and A. K. Tagantsev. Effect of mechanical boundary conditions on phase diagrams of epitaxial ferroelectric thin films. *Phys. Rev. Lett.*, 80:1988–1991, Mar 1998. doi: 10.1103/PhysRevLett.80.1988. URL http://link.aps.org/doi/10.1103/PhysRevLett.80.1988.

[18] M. Dawber, N. Stucki, C. Lichtensteiger, S. Gariglio, P. Ghosez, and J.-M. Triscone. Tailoring the properties of artificially layered ferroelectric superlattices. *Advanced Materials*, 19(23):4153–4159, 2007. ISSN 1521-4095. doi: 10.1002/adma.200700965. URL http://dx.doi.org/10.1002/adma.200700965.

[19] Dillon D. Fong, G. Brian Stephenson, Stephen K. Streiffer, Jeffrey A. Eastman, Orlando Auciello, Paul H. Fuoss, and Carol Thompson. Ferroelectricity in ultrathin perovskite films. *Science*, 304(5677):1650–1653, 2004. doi: 10.1126/science.1098252. URL http://www.sciencemag.org/content/304/5677/1650.abstract.

[20] M. Dawber, C. Lichtensteiger, M. Cantoni, M. Veithen, P. Ghosez, K. Johnston, K. M. Rabe, and J.-M. Triscone. Unusual behavior of the ferroelectric polarization in $pbtio_3$/$srtio_3$ superlattices. *Phys. Rev. Lett.*, 95:177601, Oct 2005. doi: 10.1103/PhysRevLett.95.177601. URL http://link.aps.org/doi/10.1103/PhysRevLett.95.177601.

[21] J. Sinsheimer. Enhanced piezoresponse via engineered polarization rotation in a ferroelectric superlattice. *unpublished*, 2012.

[22] P. Zubko, N. Jecklin, A. Torres-Pardo, P. Aguado-Puente, A. Gloter, C. Lichtensteiger, J. Junquera, O. Stphan, and J.-M. Triscone. Electrostatic coupling and local structural distortions at interfaces in ferroelectric/paraelectric superlattices. *Nano Letters*, 12(6):2846–2851, 2012. doi: 10.1021/nl3003717. URL http://pubs.acs.org/doi/abs/10.1021/nl3003717.

[23] HD MEGAW. REFINEMENT OF STRUCTURE OF BATIO3 AND OTHER FERROELECTRICS. *ACTA CRYSTALLOGRAPHICA*, 15(OCT):972–&, 1962. ISSN 0108-7673. doi: {10.1107/S0365110X62002571}.

[24] G. Binnig, H. Rohrer, Ch. Gerber, and E. Weibel. Surface studies by scanning tunneling microscopy. *Phys. Rev. Lett.*, 49:57–61, Jul 1982. doi: 10.1103/PhysRevLett.49.57. URL http://link.aps.org/doi/10.1103/PhysRevLett.49.57.

[25] G. Binnig, C. F. Quate, and Ch. Gerber. Atomic force microscope. *Phys. Rev. Lett.*, 56:930–933, Mar 1986. doi: 10.1103/PhysRevLett.56.930. URL http://link.aps.org/doi/10.1103/PhysRevLett.56.930.

[26] Brian J Rodriguez, Clint Callahan, Sergei V Kalinin, and Roger Proksch. Dual-frequency resonance-tracking atomic force microscopy. *Nanotechnology*, 18(47): 475504, 2007. URL http://stacks.iop.org/0957-4484/18/i=47/a=475504.

[27] P. Paruch, T. Tybell, and J.-M. Triscone. Nanoscale control of ferroelectric polarization and domain size in epitaxial pb(zr[sub 0.2]ti[sub 0.8])o[sub 3] thin films. *Applied Physics Letters*, 79(4):530–532, 2001. doi: 10.1063/1.1388024. URL http://link.aip.org/link/?APL/79/530/1.

[28] Ji Young Jo, Pice Chen, Rebecca J. Sichel, Sara J. Callori, John Sinsheimer, Eric M. Dufresne, Matthew Dawber, and Paul G. Evans. Nanosecond dynamics of ferroelectric/dielectric superlattices. *Phys. Rev. Lett.*, 107:055501, Jul 2011. doi: 10.1103/PhysRevLett.107.055501. URL http://link.aps.org/doi/10.1103/PhysRevLett.107.055501.

[29] C. S. Ganpule, A. L. Roytburd, V. Nagarajan, B. K. Hill, S. B. Ogale, E. D. Williams, R. Ramesh, and J. F. Scott. Polarization relaxation kinetics and 180° domain wall

dynamics in ferroelectric thin films. *Phys. Rev. B*, 65:014101, Nov 2001. doi: 10.1103/PhysRevB.65.014101. URL http://link.aps.org/doi/10.1103/PhysRevB.65.014101.

[30] Almudena Torres-Pardo, Alexandre Gloter, Pavlo Zubko, Noémie Jecklin, Céline Lichtensteiger, Christian Colliex, Jean-Marc Triscone, and Odile Stéphan. Spectroscopic mapping of local structural distortions in ferroelectric $pbtio_3/srtio_3$ superlattices at the unit-cell scale. *Phys. Rev. B*, 84:220102, Dec 2011. doi: 10.1103/PhysRevB.84.220102. URL http://link.aps.org/doi/10.1103/PhysRevB.84.220102.